A Final Report on

The Electrodeposition of Rhenium and Its Alloys

Grant No. FA9550-10-1-0520

Authors
Prof. Shelton Ray Taylor, PI
College of Technology
University of Houston
srt@uh.edu

Prof. Noam Eliaz, Co-Inv.
Faculty of Engineering
Tel Aviv University
neliaz@tauex.tau.ac.il

Prof. Eliezer Gileadi, Co-Inv.
School of Chemistry
Tel Aviv University
gileadi@post.tau.ac.il

Report Date
18-09-2015

Reporting Period Start Date:
September 15, 2010

Reporting Period End Date:
September 14, 2015

Sponsoring Agency
Air Force Office of Scientific Research (AFOSR)
875 Randolph Street
Suite 325, Room 3112
Arlington, VA 22203

Program Manager
Dr. Ali Sayir

Table of Contents

1.0 ABSTRACT

The electrodeposition of rhenium (Re) and Re alloy (Re-M) coatings is a low cost and efficient means to produce an important coating that can improve the corrosion, wear, and high temperature oxidation resistance of critical assets. The objectives of this research are to develop an understanding of the mechanism that governs the electrodeposition of Re and its alloys. This understanding will be used to optimize a near-room-temperature, aqueous, non-toxic electro- and electroless deposition process for Re and binary and ternary alloys (Re-M, Re-M-N) on substrates relevant to the Department of Defense. These objectives have been accomplished through a 5 year, 3 investigator, bi-national collaboration between researchers at the University of Houston and Tel Aviv University. In addition to providing significant advancement into the understanding of electro- and electroless deposition of a strategically important material, we have gained insight into the complex interactions between bath constituents and the substrate. Some of these interactions were first predicted by new quantum level computational methods developed within this project, and then verified experimentally. The non-toxicity of the bath chemistry combined with the strategic qualities of rhenium make the results of this research timely and essential.

Since the last report (year 4), we have examined: (1) the effect of plating variables on the electrodeposition of the ternary alloy, Re-Ir-Ni, (2) the role of pulse plating variables on Re-Ni electrodeposits, (3) electroless plating of Re-Fe, Re-Ni, and Re-Co, and (4) the interaction between perrhenate, nickel, and citric acid using quantum chemistry calculations and spectroscopic methods. For the Re-Ir-Ni system, we found that the Faradaic efficiency (FE), partial current densities for deposition of the three metals, and deposition rate increase as the pH is increased from 2.0 to 8.0 (at T=70°C). The highest Re-content is obtained at pH = 2.5, in a 82Re-8Ir-10Ni alloy (at%). A decrease of pH, to 2.0, results in the formation of a 70Re-18Ir-12Ni alloy that, while containing less Re and slightly more Ni, may provide better high-temperature oxidation resistance due to the higher Ir content. At pH = 2.0, the coating consists of an amorphous phase, and no surface cracks are observed. When the pH is raised to 4.0 and above, crystalline phases (including hydrides) form, and both columnar crystals and micro-cracks are observed.

In our pulse plating effort, we found that the surface morphology diagram is divided into three regions: (1) smooth coatings were produced for all tested on-times (10-700 ms) when peak current densities were below –30 mA cm^{-2} since $j_p < j_{lim}$, (2) j_p = –30 to –50 mA cm^{-2}, t_{on} = 10 to 100 ms, since $j_{lim} < j_p < j_{pL}$, smooth coatings were observed, however increasing either j_p or t_{on} led to rough coatings, and (3) rough coatings when long on-times were coupled with high peak current densities, $j_p > j_{pL}$. When j_p exceeds j_{pL}, the system experiences increased hydrogen evolution, which may give rise to molecular hydrogen attached to the surface leading to rougher deposits. In addition, the concentration of rhenium oxides decreases relative to that of Re when either the duty cycle or peak current density decreases. The absence of *fcc*-Ni reflections (200) and (311) in the smooth samples is accompanied by a doubling of the Re-content in these

samples as compared with rough deposits. In addition, the smooth deposits contain evidence of a solid solution of Re in *hcp*-Ni.

In our electroless deposition study of Re-Me (Me = Ni, Co, Fe), we were able to prepare uniform films of Re-Ni and Re-Co alloys with Re-contents of 78 at.% and 65 at.%, respectively. In addition, we were able to demonstrate the catalytic effect of iron-group metals on reduction. The Re-Me surface accelerates DMAB oxidation compared to copper, therefore the overall rate of the auto-catalytic reaction on an alloy substrate is significantly higher than on Cu substrate, except in the case of Re-Co. The deposition rate of Re-Fe was found to be significantly lower, probably due to the ability of the ion to oxidize and dissolve most of the metallic iron. The heterogeneous reaction on the surface of all deposited Re-Me alloys during their electroless deposition is controlled by charge-transfer rather than by mass transport of the reducing agent and metal ions.

Using quantum level computations (Gaussian 09), we were able to see interactions between the bath components that showed unexpected benefits, particularly with the addition of energy. Computational evidence shows that Re, Ni, and citric acid can interact and introduce new oxidation and reduction states of the metal cations. The chemical interactions between perhennate, Ni, and citric acid was verified using Raman spectroscopy of solid constituents reacted by mechanical grinding. The interaction appears to be dominated by citrate and less by Ni. The interactions are reduced by the presence of protons.

2.0 PROJECT SUMMARY

Rhenium (Re) and Re alloy (Re-M) coatings provide an important means to improve the corrosion, wear, and high temperature oxidation resistance of critical assets. Unlike chemical vapor deposition, electrodeposition is an efficient, low cost method to apply high quality Re and Re-M coatings on complex substrates. However, neither the fundamentals of Re electroplating nor the relevant processing variables are properly understood. The objectives of this research were to develop the mechanism that governs the electrodeposition of Re and its alloys. This understanding was used to optimize a near-room-temperature, aqueous, non-toxic electro- and electroless deposition process for Re and binary (Re-M) and ternary (Re-M-N) alloys on substrates relevant to the Department of Defense. These objectives were accomplished in a 5 year, 3 investigator, bi-national collaboration that combines experience in fundamental electrochemistry and alloy electrodeposition of researchers at Tel Aviv University (TAU) with the expertise in coatings science and high throughput (HT) electrochemistry of researchers at the University of Houston (UH).

The two interacting components of research, mechanistic studies and process optimization, were applied to electrodeposited and electrolessly deposited Re, Re-M, and Re-M-N alloys (*e.g*., M, N = Ni, Ir, Rh, W) on Cu substrates. An additional research phase optimized a bath for Re and Re-M deposition on a substrate material of interest to the DoD, *e.g*., carbon-carbon composite. The thermodynamic- and kinetic-based methods developed by TAU to understand the mechanism of W-Ni electrodeposition provided guidance to the HT electrodeposition methods developed by UH to optimize the deposition processes of Re and Re alloys. Mechanistic findings from process optimization studies at TAU and Density Functional Theory-based calculations at UH guided the HT optimization studies at UH. In materials-based studies, TAU analyzed the hardness, microstructure, crystal structure, and composition of resulting electro-deposits.

This research project combined science and engineering in an inter-dependent manner. Graduate students and post graduate researchers were immersed into a research topic where the results, whether mechanistic or process engineering, had a tangible technological need and impact. The high temperature (3180^{o}C), high wear, and corrosion resistance of Re and Re-alloys make it a critical material for strategic components in numerous industries (defense, aerospace, chemical, nuclear, biomedical, *etc.*). The researchers worked on a team known for innovation using state-of-the-art methods designed for discovery.

Of equal importance to the science and innovation was the cooperation between the two groups of scientists in the US and Israel. This collaboration strengthened the scientific cooperation between our countries to the benefit of both. The technologies developed under this project have a strong potential to create new jobs for young scientists and form the basis of a new industry.

3.0 STATEMENT OF WORK

The objectives of this research were to understand the mechanism and the factors that influence the deposition of Re and its alloys. Two types of alloys were studied: binary systems (Re-M, *e.g.*, M = Ni, Co, Fe) and a ternary system Re-M-N that includes some of the noble (*e.g.*, N = Pt, Ir, Os) and refractory metals (*e.g.*, W, Mo). The complexity of these systems should not be underestimated. Multiple parallel electrochemical reactions occur in a bath chemistry containing many different complexes having a spectrum of stability states.

These objectives were accomplished through a 5 year, 3 investigator, bi-national collaboration that combines experience in fundamental electrochemistry and alloy electrodeposition of researchers at TAU with the expertise in coatings science and high throughput (HT) electrochemistry of researchers at the UH. There were two interacting components of research; mechanistic studies and process optimization. Initial studies on electrodeposited Re evolved into Re-M, and then Re-M-N alloys on Cu substrates. Research also developed the mechanistic and process understanding for electroless deposition of Re and Re alloys. An additional research phase optimized a bath for Re and Re-M deposition on a material and shape of interest to the DoD.

TAU used thermodynamic and kinetic-based methods to understand the mechanism of Re and Re alloy electrodeposition These results provided guidance to the high throughput (HT) electrodeposition methods developed by UH to optimize the deposition processes of Re and Re alloys. In turn, the HT methods of UH were used to guide and confirm mechanistic determinations by TAU. Fully developed HT methods will allow full factorial design to optimize bath chemistry, additives, operating conditions, and pulse plating regime. In detailed materials studies TAU analyzed the hardness, microstructure, crystal structure, and composition of resulting electrodeposits using SEM, EDX, XRD, and TEM. UH screened the HT coating outcomes with a tiered assay system using the open-circuit potential, electrochemical impedance, bending/adhesion, and bending/heating/quench/adhesion.

The proposed research has helped to understand a new uncharted group of super-alloy electrodeposits and electroless deposits of a material with extremely high melting point, high wear, and excellent corrosion resistance. UH and TAU team have expertise in science and engineering needed to develop and optimize Re and Re-alloy coatings. But the development of this science into a useable technology will require guidance from the DoD. The coatings developed in this research have the potential to extend the service-life of critical DoD assets, thus increasing mission readiness, safety, and asset availability.

4.0 SIGNIFICANT OUTCOMES

4.1 Mechanistic findings from process optimization studies

Details on experimental methods, results, and interpretation can be found in the manuscripts listed in Section 9.0.

4.1.1 The electrodeposition of Re-M alloys

Initial studies at TAU examined the effect of bath chemistry on Re-M deposition. The plating process was quantified in terms of Faradaic efficiency (FE), atomic % content of Re within the electrodeposit, and partial currents. The Re-M alloys examined were those where M was a transition metal, M = Ni, Fe, or Co. Electrodeposits were formed galvanostatically, a conventional method used within industry. The plating bath consisted of ammonium perrhenate, nickel or cobalt sulfamate, or iron sulfate, citric acid, and magnesium sulfamate. Rhenium contents as high as 93 atom % and FE values as high as 96% were attained in different solutions.

.

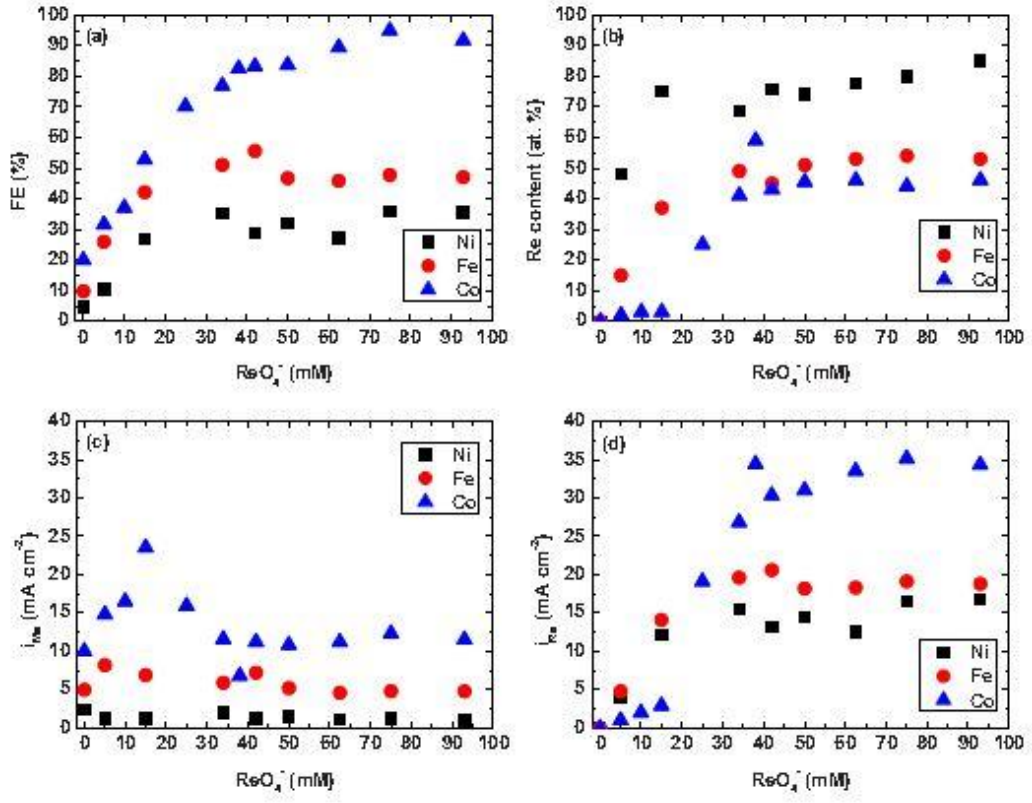

Figure 1.1. The dependence of (a) the FE, (b) Re content in the deposit, (c) the partial current density of M, and (d) the partial current density of Re on ReO_4^- concentration. The analytical concentrations of M and citric acid were 93 and 343 mM, respectively. Plating was conducted for 1 h at 70°C, 50 $mAcm^{-2}$, and pH 5.0 $\pm$ 0.1.

All plating baths consisted of consisted of ammonium perrhenate, citric acid, and a salt of one of the iron group metals. Figure 1.1a and b show the effect of the ReO_4^- concen-

tration on the FE and Re content in the deposit, respectively. The dependence of the partial current densities of M and Re on the concentration of the ReO_4^- ion is shown in Figure 1.1c and d, respectively. The concentrations of M and citric acid in the bath were 93 and 343 mM, respectively.

The effect of increasing the concentration of ReO_4^- above 34 mM on the FE and the Re content in the deposit is rather small, possibly within the experimental error, in Re–Ni and Re–Fe alloys. Considering the partial current densities for deposition, a similar trend was observed for the second metal. The partial current density for Re alloyed with Ni or Fe is also nearly independent of the concentration of ReO_4^- in solution, above a concentration of 34 mM. However, in Re–Co alloys, the partial current density for Re deposition increases significantly with the concentration of perrhenate, reaching a nearly constant value at approximately 60 mM ReO_4^-.

When the ReO_4^- concentration in solution was lower than 34 mM, the FE, the Re content in the deposit, and the partial deposition current density of Re increased with the increasing concentration of ReO_4^- in all three systems. As for the partial deposition current density of the second metal, in Ni and Fe it seems to be rather constant, while in Co it exhibits a local maximum at a ReO_4^- concentration of about 15 mM. When considering the partial current densities, it should be kept in mind that the deposition of one of the iron-group metals requires only two electrons, while that of Re requires seven electrons. Thus, equal partial current densities correspond to an atomic concentration ratio of Re:M = 1:3.5 in the deposited alloy.

The effect of deposition time was studied for t = 20–100 min under otherwise constant conditions, as shown in Figure 1.2. The data for the three iron-group metals follow linear relationships and extrapolate to zero thickness at t = 0. This shows that the rate of deposition was uniform, independent of time. For the particular bath composition used in these series of experiments (34 mM ReO_4^-, 93 mM M^{2+}, and 343 mM Cit), the rate of deposition was quite different for the three alloying elements, namely 10, 14, and 24 μm h^{-1} for Re–Ni, Re–Fe, and Re–Co, respectively.

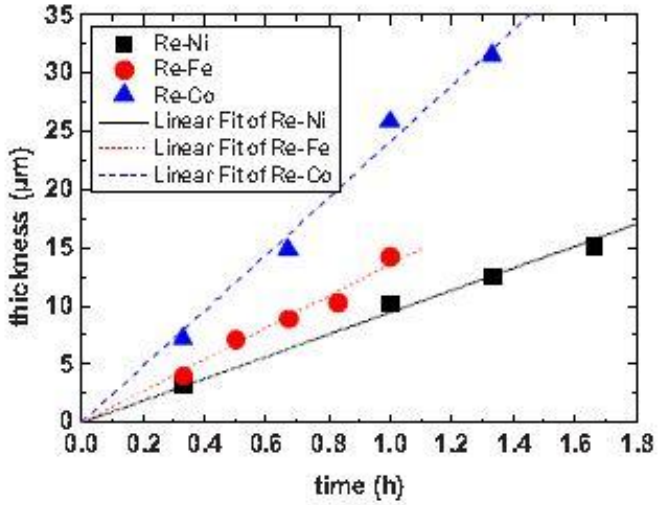

Figure 1.2. Calculated thickness vs time for baths containing 93 mM iron-group metal salt, 34 mM ammonium perrhenate, and 343 mM citric acid. The linear fit yields deposition rates of 24, 14, and 10 μmh^{-1} for Re–Co, Re–Fe, and Re–Ni, respectively.

Figure 1.3 shows the same parameters as Figure 1.1, as a function of the concentration of each of the iron-group metals in solution, keeping the concentration of ReO_4^- and citric acid constant. It can be seen that the FE increases with the concentrations of each of the alloying elements (Figure 1.3a), whereas the Re content in the alloy decreases (Figure 1.3b). In Figure 1.3c and d, it is evident that both the partial current density of M and that of Re increase as the concentration of the M ion concentration in the bath is increased.

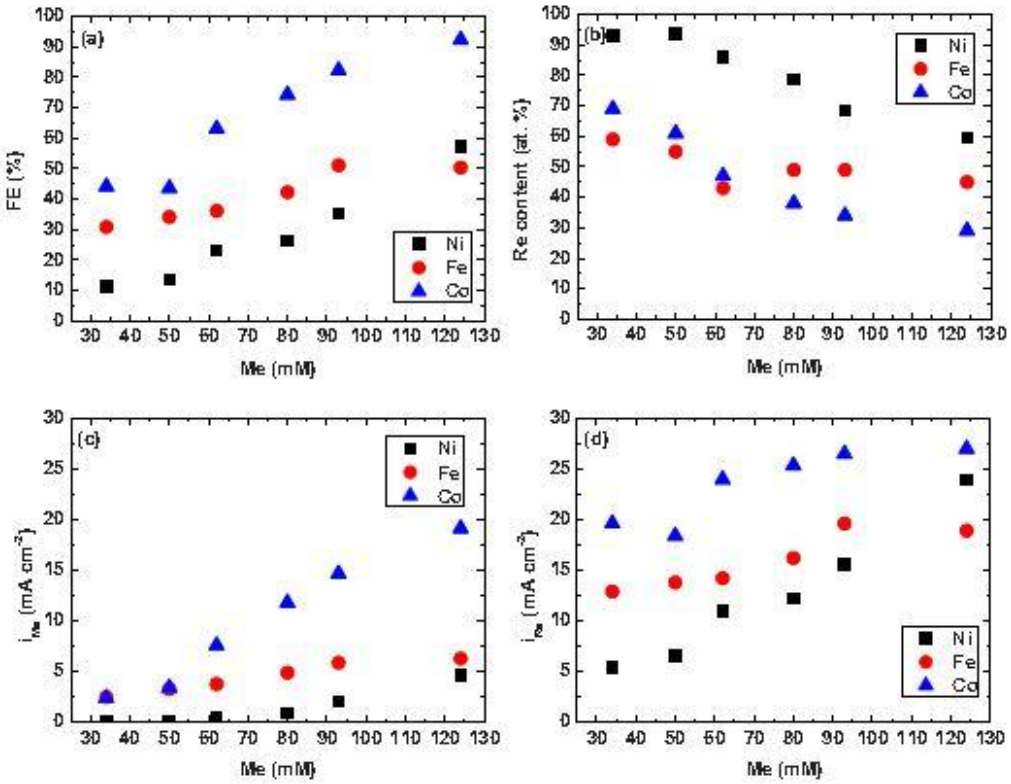

Figure 1.3. The dependence of (a) the FE, (b) Re content in the deposit, (c) the partial current density of M, and (d) the partial current density of Re on the concentration of M. The concentrations of ReO_4^- and citric acid were 34 and 343mM, respectively. Plating was conducted for 1h at 70°C, 50 $mAcm^{-2}$, and pH 5.0 $\pm$ 0.1.

The effect of the concentration of citrate on the partial current densities of the iron-group metal and for Re is shown in Figure 1.4a and b, respectively. The partial current density for the deposition of Fe is independent of the citrate concentration, while that of Ni and Co depends on it in different ways, as shown in these figures.

Figure 1.5 shows the surface morphology of coatings made in this phase of research. The typical surface morphology of Re–Fe alloy coating is uniform with no visible cracks. The typical surface morphologies of Re–Co and Re–Ni alloys coatings are uniform, but each contains a net of microcracks, which most likely result from internal stress. The crack width is typically in the range of a few hundreds of nanometers. Subsequent effort

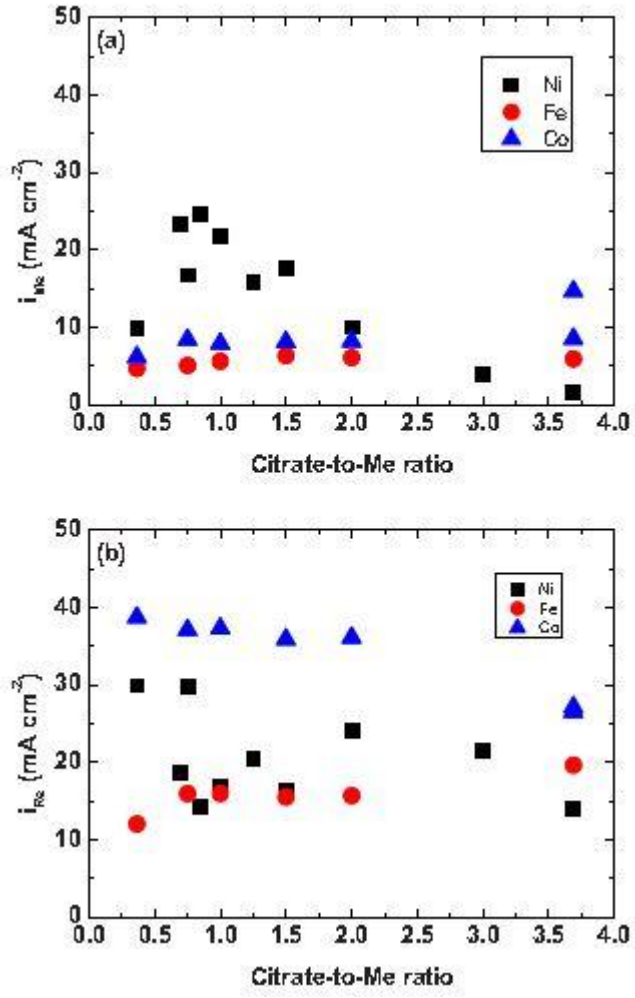

Figure 1.4. The partial deposition current densities of the (a) iron-group metal and (b) Re as a function of the citrate-to-M ratio. The ReO_4^- and M concentrations were 34 and 93 mM, respectively.

later in the research program was able to eliminate these cracks through the use of stress relievers.

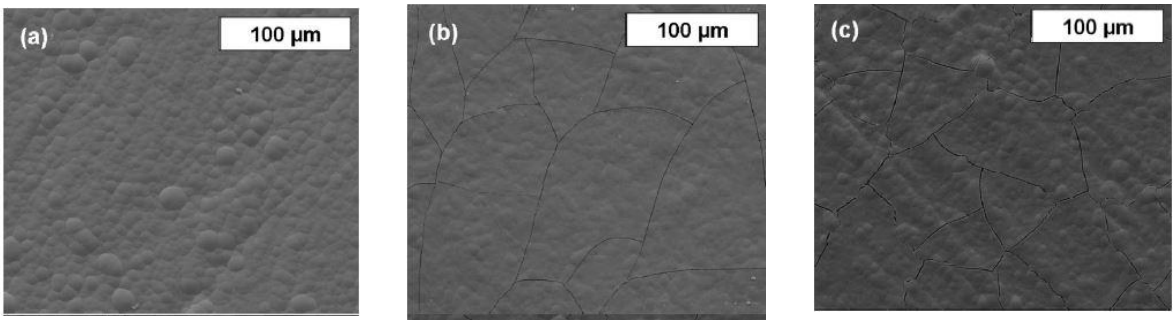

Figure 1.5. Scanning electron microscopy images revealing the typical surface morphologies of (a) Re–Fe, (b) Re–Co, and (c) Re–Ni alloys.

In previous studies, the induced codeposition of tungsten with nickel was analyzed. The main objective was to suggest a mechanism that could explain the synergistic effect of Ni and W and be consistent with all experimental observations. When a salt of Ni was added to the plating bath, alloys of Ni–W having a wide range of concentrations could

be formed. A similar behavior was found when Ni was replaced by Fe or by Co. The conclusion was that this synergism was a result of the unique solution chemistry used, which included WO_4^{2-}, Ni^{2+}, and Cit^{3-}. In that system adjusted to pH 8.0 $\pm$ 0.1, Ni^{2+} forms a complex with Cit^{3-} and, somewhat surprisingly, the WO_4^{2-} ion also forms a complex with Cit^{3-}, according to the reactions

$$Ni^{2+} + Cit^{3-} \rightarrow [(Ni)\,(Cit)]^{-} \quad (1)$$

and

$$WO_4^{2-} + Cit^{3-} + H_2O \rightarrow [(WO_4)\,(Cit)(H)]^{4-} + (OH)^{-} \quad (2)$$

While nickel can be electrodeposited from both species in Eq. 1, tungsten cannot be deposited from either of the species that contain it in Eq. 2.

The two complexes formed in Eq. 1 and 2 combine to form a complex containing both metals, according to the equation

$$[(Ni)(Cit)]^{-} + [(WO_4)(Cit)(H)]^{4-} \rightarrow [(Ni)(Cit)(WO_4)(H)]^{2-} + (Cit)^{3-} \quad (3)$$

It was concluded that the precursor for the deposition of the Ni–W alloy is the complex ion containing both metals. This is expected to yield an alloy consisting of equal atomic concentrations of Ni and W. However, Ni can also be deposited from its complex with citrate, while the only precursor for the deposition of W is the ion on the right-hand side of Eq. 3. As a result, the concentration of W in the alloy was usually less than 50 atom %. Indeed, it required a large excess of the WO_4^{2-} ion and fine-tuning of the concentration of the citrate to produce a Ni/W = 1/1 alloy. One of the observations supporting this mechanism was that the synergistic effect between the two metals was mutual. Thus, increasing the concentration of Ni^{2+} in solution increased the partial current density for the deposition of W, and, similarly, increasing the concentration of WO_4^{2-} in solution increased the partial current density for the deposition of Ni^{2+}. This is consistent with Eq. 3 because increasing the concentration of either metal would lead to an increase in the concentration of the complex.

The most stable ion of Re in solution is ReO_4^{-}, which is isoelectronic with WO_4^{2-}.Hence, similarities in the electrochemical properties of the two metals is expected, although their chemistries are different. We have found some similarities in the sense that the addition of Ni^{2+} enhanced the rate of deposition of both Re and W. But that is where the similarity ends. Re could be deposited from a solution of NH_4ReO_4, but at a low FE, producing rather poor films. However, the effect of addition of Ni^{2+} ions to the bath is much more dramatic than that in W. Equal molar concentrations of $Ni^{2+}$and ReO_4^{-} (34 mM) led to about 93 atom % of Re in the deposited film, but the FE was only 11%. Increasing the concentration of $Ni^{2+}$to 124 mM led to lowering the concentration of Re to 60 at%, while the FE rose above 57%, as shown in Figure. 1.3a and b. Clearly, the influence of Ni on the deposition of Re must follow a different path than that on W. Thus, forming an alloy that contains 50 atom % W required a ratio of Ni^{2+}/WO_4^{2-} = 1/10 in solution, while the

same concentration of Re in the alloy is reached when the ratio is Ni^{2+}/ReO_4^- = 3.6/1. In Ni–W, the highest concentration of W in the alloy was 50 at%, with some indication that an alloy corresponding to the composition of NiW_2 may have been formed at very low FE. This could be explained by assuming that a somewhat similar precursor for the deposition of the alloy, namely $[(N)(WO_4)(H)_2(Ci)]^{3-}$ existed. However, assuming the same mechanism for Ni–Re deposition, an alloy containing, for example, 90 at% Re should have a precursor comprising nine ions of $ReO4^-$ and only one of Ni^{2+}, which is totally improbable. The strong influence of the addition of Ni^{2+} to the solution, even though it is incorporated in the deposit only as a minor component, points to the role of Ni^{2+} as a **catalyst**, not as a component of a precursor from which the alloy is deposited.

An initial survey of different metals to be plated as an alloy with Re showed that Ni, Co, and Fe have the strongest influence on the rate of deposition of the alloy. Among the other metals tested - Mn, Zn, Sn, Cu, and Ce - only Sn had a significant effect, but the behavior of the Sn–Re alloy was very different from that of the three iron-group metals, as will be reported elsewhere. Although Ni, Co, and Fe seem to behave in a similar manner, probably following the same mechanism, in some aspects they are different. In Figure 1.2, the rate of deposition of the Re alloy with each of the three metals was shown. For each metal, the rate of deposition is independent of time over the range of 20–100 min, but the calculated thickness (assuming bulk density) showed the highest rate of 24 $\mu m\ h^{-1}$ for Co, the lowest rate of 10 $\mu m\ h^{-1}$ for Ni, and a value of 14 $\mu m\ h^{-1}$ for Fe. This implies that a first step, which we believe is the reduction of the divalent metal on the surface, is the rate-determining step in the deposition of the alloy. For example:

$$Co^{2+} + 2e_M^- \rightarrow Co_M{}^0 \qquad (4)$$

The metallic Co formed in this step reduces the ReO_4^- ion, as shown in Eq. 5 below.

$$CoM^0 + ReO_4^- + H_2O \rightarrow Co^{2+} + ReO_3^- + 2(OH)^- \qquad (5)$$

In Figure 1.1b, the most striking result is that the Re content in the alloy is almost independent of the concentration of the ReO_4^- ion in solution at concentrations above 34 mM. The FE was also independent of the ReO_4^- concentration at these concentrations. This is consistent with the notion that reduction of the ReO4− ion is not the rate-determining step in the present system, as suggested above, based on the different rates of deposition of the alloy with the three iron-group metals (Figure 1.2). The increase in the FE, Re content, and partial deposition current density of Re with increasing ReO_4^- concentration below 34 mM can be attributed to mass-transport limitation of the ReO_4^- ion.
While the FE is a definite measure of the rate of hydrogen evolution (assuming that it is the only side reaction in this system), the Re content in the alloy is less definitive. For example, its increase could result either from an increase in its rate of deposition or from a decrease in the rate of deposition of the second metal. Thus, more important are the partial current densities shown in Figure 1.1c and d for each of the iron-group metals and for Re, respectively. The partial current densities for deposition of the iron-group metal are almost independent of the concentration of ReO_4^- in solution in Ni and

Fe. In Figure 1.1d, the partial current for the deposition of Re, for perrhenate concentrations higher than 34 mM, depends only little on its concentration in solution. Considering that the rate of deposition of the Co–Re alloy in solution with a relatively high concentration of ReO_4^- is about twice as high as that of the Ni–Re and Fe–Re alloys, it is easy to see that the deposition of the Co–Re alloy is most affected by mass-transport limitation. Moreover, the behavior of the partial deposition current density of Co differs from that of Ni and Fe and exhibits a local maximum at a ReO_4^- concentration of about 15 mM, which cannot be explained at this stage.

The effects of the concentration of the iron-group metal, while keeping the concentration of ReO_4^- constant, are shown in Figure 1.3. In this case, the behavior observed is as expected, and the interpretation is straightforward. The FE for all three iron-group metals increases with increasing concentration (Figure 1.3a), while the Re content in the alloy decreases (Figure 1.3b). This may be because Re is a much better catalyst for hydrogen evolution than any of the three iron-group metals, so that lowering the proportion of Re in the alloy can be expected to lead to a decrease in the rate of hydrogen evolution and, hence, to an increase in the FE. However, it should be kept in mind that the experiments were carried out under galvanostatic conditions, so an increase in the partial current density of Re and of the iron-group metal should result in a decrease in the partial current density for hydrogen evolution. The partial current density for all the iron-group metals increased with an increase in their concentration in solution, as expected (Figure 1.3c). However, the partial current density of Re deposition also increased, although the Re content in the alloy decreased. Thus, in contrast to the Ni–W system, the synergism here is one sided; increasing the concentration of ReO_4^- does not increase the partial current density for the deposition of the iron-group metal, pointing again to a different mechanism governing the deposition of the Re alloys.

The effect of increasing the concentration of the Cit^{3-} ion while keeping the concentration of both metals constant was also investigated. The partial current density for Co deposition increased moderately with increasing concentration of citrate, whereas that of Fe was essentially independent of it. The partial current density for Re deposition increased when Fe was the second metal and decreased when it was Co. The data for Ni were rather complex, showing a maximum in the current density for Ni deposition and a corresponding local minimum for Re deposition, as shown in Figure 1.4a and b, respectively. These results probably depend on the different complexes of each of the elements with citrate, but some of the values of the stability constants for the complexes needed for a quantitative analysis are not available. Suffice it to say that the most satisfactory results, from the point of view of the quality of the electrodeposited film, as observed by SEM studies, were obtained at the highest concentration of Cit^{3-} used in this study (343 mM). The role of citrate is probably to sequester the ions of the iron-group metal, slowing down their rate of deposition. This is most likely the reason that the concentration of ReO_4^- has very little effect on the rate of the overall process of alloy formation, while this rate is sensitive to the concentration of the iron-group metals and shows significant differences between Co, Ni, and Fe.

Proposed mechanism.— Based on the experimental data, the following mechanism is proposed to explain the effect of Ni^{2+}, Co^{2+}, and Fe^{2+} ions on the rate of deposition of the respective alloy with Re. The first step is the electrodeposition of the divalent ion, as given by Equation 4. The next step is the chemical reduction of ReO_4^- (Equation 5). Because the ReO_4^- ion is the most stable ion of Re in solution, it is very difficult to deposit metallic Re from it directly. However, its chemical reduction to the five-valent state may make it easier to reduce it further electrochemically to the metallic state

$$ReO_3^- + 5e_M^- + 3H_2O \rightarrow Re_M^0 + 6(OH)^- \quad (6)$$

An alternative path could be the further chemical reduction of ReO_3^- in several steps to form metallic Re, but we consider this a less likely mechanism.

4.1.2 The effect of bath additives, potentiostatic plating and pulse plating

The effects of different deposition parameters, such as applied potential in potentiostatic deposition, or cathodic pulse current density and duty cycle in pulse plating, on the Faradaic efficiency (FE), Re-content in the deposit, partial deposition current densities, and the structure, surface morphology and cracking of the coatings, were studied. The following findings were obtained:

- Crack-free Re-Co and Re-Ni alloys were formed by pulse plating and by potentiostatic electrodeposition, with Re-contents in the deposits up to 82 at.%, and FE as high as 76%.
- In pulse plating, reverse pulse shape was found most useful for obtaining crack-free Re-Co alloys, while cathodic pulse plating shape was found helpful for obtaining crack-free Re-Ni alloys.
- In potentiostatic deposition, as the overpotential was increased, the average crack size also increased.
- In the case of Re-Ni alloys, as the pulse current or the duty cycle were increased, the average crack size was increased.

Figure 2.1 presents ESEM (Environmental SEM) images of: (a) crack-free Re-Co coating obtained by potentiostatic deposition at –0.6 V, (b) crack-free Re-Co coating obtained by reverse pulse plating, (c) Re-Ni coating obtained by reverse pulse plating, and (d) crack-free Re-Ni coating obtained by pulse plating. The details of the precise methods and results can be found in the publications listed in Section 9.0.

Most combinations of organic bath additives did not have benefit. A combination of vanillin, sodium lauryl sulfate, and gelatin, and equal concentrations of Ni^{2+} and ReO_4^- yielded a coating with ~100 at.% Re, FE = 15.4%, fine grains, and essentially no cracking. As minimal cracking is associated with maximal Re-content and minimal FE, the cracking is most likely the outcome of residual stresses due to crystallographic mismatch between Re-rich and Ni-rich phases, and **not** due to hydrogen absorption.

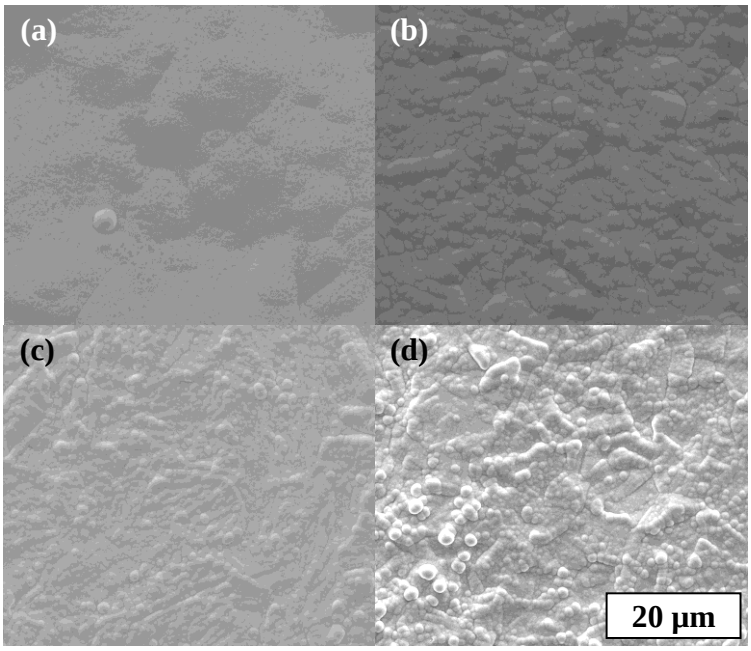

Figure 2.1. ESEM images of: (a) crack-free Re-Co coating obtained by potentiostatic deposition at –0.6 V, (b) crack-free Re-Co coating obtained by reverse pulse plating, (c) Re-Ni coating obtained by reverse pulse plating, and (d) crack-free Re-Ni coating obtained by pulse plating.

4.1.3 The initial stages of Re-Ni electrodeposition (0.05–60s)

The effect of deposition time on the Faradaic efficiency (FE) and the atomic percent (at%) of Re in the coating was examined using three citrate containing electrolytes. All three electrolytes contained 100 mM citric acid.

Electrolyte #	$Ni(SO_3NH_2)_2$ (mM)	NH_4ReO_4 (mM)
1	-	34
2	94	-
3	94	34

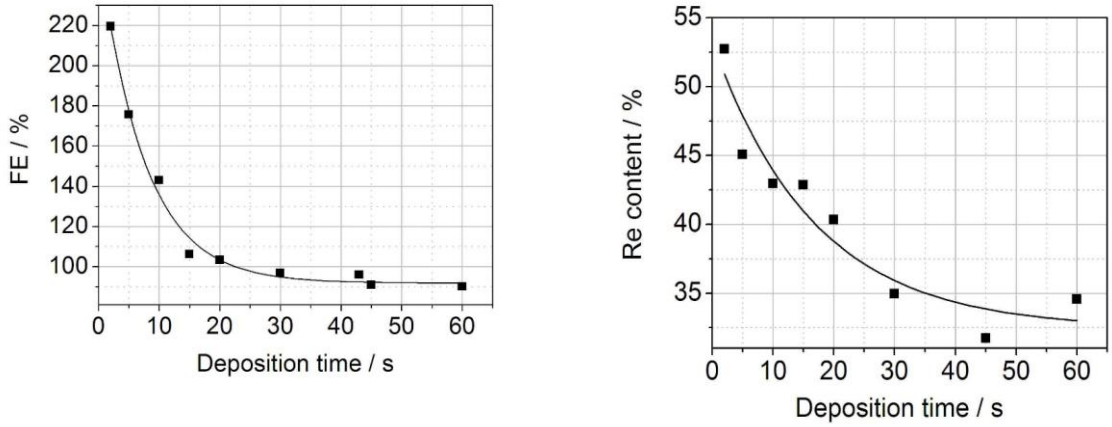

Figure 3.1. The Faradaic Efficiency and Re content as a function of deposition time for Electrolyte #3 at 70^o C and 50 mA/cm^2. Each point is the average of three independent measurements. The line is fit by least square fitting.

The rate of alloy deposition and the apparent FE of the deposition process were much higher than those for the deposition of either pure Re or pure Ni. As seen in Figure 3.1, anomalous values of the FE, well above 100%, were observed at short deposition times. The values of the FE decreased with the deposition current density and with deposition time, reaching a steady-state value after about 60 s. The Re-content in the Re-Ni deposits decreased with deposition time in a similar manner.

Experiments of anodic stripping charge vs. deposition time showed linear behavior for different deposition current densities and crossed the ordinate above zero. The anodic stripping charge at a deposition time equal to zero increased with current density. These dependences and anomalous FE confirm that a chemical reaction is taking place in parallel with the electrochemical process at short times. Based on these findings we have suggested the catalytic character of the chemical and electrochemical reactions taking place during the deposition of Re-Ni alloys. Chemical reactions are triggered only after application of current, which causes a large shift of the potential. The changes in catalytic properties of the cathode surface with deposition time result in a decline in the rate of the chemical reactions. The citrate ions in solution play an important role in creating a parallel chemical reduction, which only occurs at high negative potentials, generated by applying a high current density.

The process is influenced by mass transport and by concentration of citric acid in the electrolytes. High Re-contents (60-65 at.%) were found in the deposits produced in stagnant electrolytes. Mass transport contributes to the increase of Re-content in the deposits produced in the electrolytes with 340 mM citric acid and contributes to its decrease in the deposits produced in the electrolytes with 100 mM citric acid. No ternary complexes consisting of ReO_4^-, Ni^{2+} and citrate were found in the electrolytes by means of conductometry, UV-Vis and Raman spectroscopy

The increased deformation of the perrhenate ions with increasing molar ratio of $NiCit^-$ /ReO_4^- was clearly shown by Raman spectroscopy, indicating one week ionic interactions. This regularity cannot explain the intensification of the deposition process with the increase of ReO_4^- concentration in the electrolyte. The induced co-deposition is found to be a catalytic process, occurring on the surface by the simultaneous reduction of ReO_4^- and $NiCit^-$, which influence each other by week interaction. Induced co-deposition of rhenium and nickel was suggested to proceed partially from the precursor adsorbed on the cathode and consisted of deformed ReO_4^- and Ni^{2+}-citrate complex ions. The deposition from this precursor led to formation of the layer catalyzing parallel deposition from perrhenate ion and Ni-citrate complex separately.

Re-Ni films were formed by electroless deposition on SiO_2 (100 nm)/Si substrates. The SiO_2 (100 nm)/Si substrate was modified by amino-terminated siloxane, in order to improve the adhesion of the Re-Ni deposits to the non-conducting SiO_2 substrate. In the next step, substrates were immersed for 3.5 h at 60-65°C in a 1% solution of APTMS (terminated with NH_2 groups) in ethanol, to form a monolayer of silane on the surface. Subsequently, the samples were rinsed in ethanol using ultrasonic agitation. After silanization, the substrates were activated by dipping into a Pd-citrate solution for

20 min. Electroless plating bath with DMAB as the reducing agent was used for Re-Ni deposition. Plating: 3.45 mM $NiSO_4$, 34.5 mM $KReO_4$, 170 mM $Na_3C_6H_5O_7$, 100 mM DMAB, pH = 9.0-9.5, T = 90-95^o C. Ultrathin (7 nm) Re-Ni layers with uniform thickness were electroless plated. Ni^{2+} is found necessary to obtain full surface coverage and thicker deposits. The process used is simple, employing silanization in ambient conditions, as opposed to the common silanization processes in either a nitrogen atmosphere or vacuum (CVD).

As-deposited Re-Ni films consist of both amorphous Ni-Re and $H_{0.57}ReO_3$ phases (based on comparison to XRD patterns reported elsewhere for powders of ReO_3 reacted with hydrogen). In the case of pure Re deposits, the same $H_{0.57}ReO_3$ phase was also detected (b). Based on Figure 3.3 (b),(c),(d) the electroless Re-Ni layers are not chemically stable in air at room temperature, and seem to be oxidized and to undergo hydrogen intercalation and consequent transformation to the $H_{0.57}ReO_3$ phase. This effect can be attributed to a high hydrogen evolution rate during deposition of high

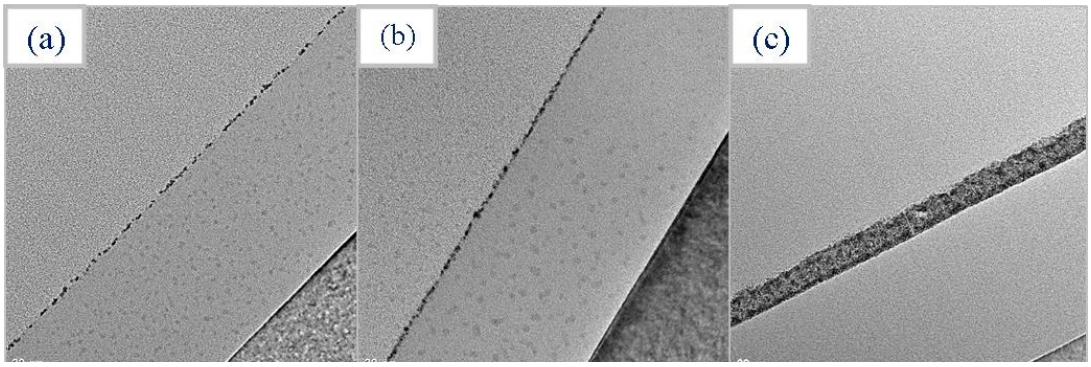

Figure 3.2. TEM cross-section images of: (a, b) Re deposit, (c) Re-Ni deposit, formed from baths containing either only potassium perrhenate or potassium perrhenate and nickel sulfate, respectively. Deposition time: (a) 15 s, (b, c) 40 s. The dark electroless coating is at the interface between two pieces of Si/SiO_2.

Re-content alloys, and thus to the absorption of hydrogen in the coating during deposition. Moreover, the fine-grained structure of the Re-Ni deposits (Figure 3.2) that are formed during deposition can also accelerate the degeneration of the coating. In order to improve the stability of such layers, thermal treatment is required. The observation of the $H_{0.57}ReO_3$ phase is interesting. It has been reported that most of the thin films of ReO_3 deposited by thermal evaporation and sputtering consist of a rhenium-hydrogen phase. This disordered H_xReO_3 phase was proposed for solid-state battery and liquid-crystal cell applications due to its high ionic and electronic conductivities. The Re-content was not uniform along the thickness of the deposit, and had a maximal value at the percolation point (also observed by resistivity measurements). Evolution of the layer from the growth of separate islands, through coalescence, percolation, and finely the formation of a complete layer. During the percolation period (points A-C, Figure 3.3), film deposition is slower than during continuous film growth. This may lead to an interesting mixture of conducting and “non-conducting” layers in microelectronic applications because it allows controllable exhibition of two opposite states at any

system. Applications for this include electrical contacts and interconnects metallization for integrated circuits where thickness and electrical conductivity are main figures of merit of the deposited metal films.

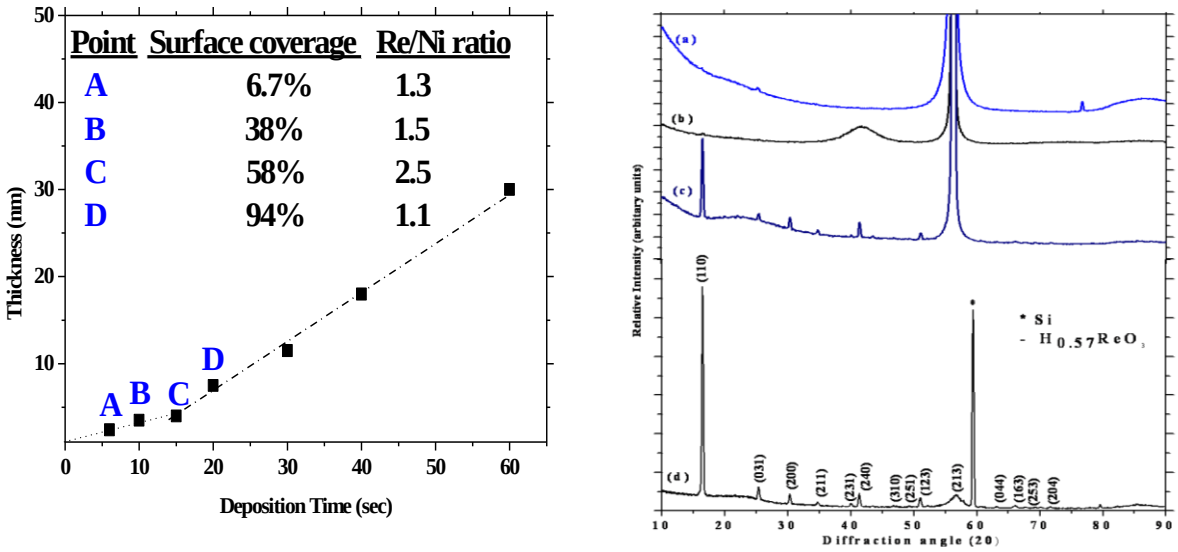

Figure 3.3. (a) Thickness of the Re-Ni films vs. deposition time. The effects of deposition time on the surface coverage and Re-to-Ni atomic ratio are also demonstrated. (b) XRD spectra of electroless plated: (a) Re, (b) Re-Ni, after 40 s of deposition. (c, d) are the diffraction patterns of sample (b) after aging in air (ambient environment) for 2 weeks and 1 month, respectively.

Anomalous values of FE, as high as 3,900%, have been observed. Both the Re-content and the FE decrease over time. Similar trends were observed for Re-Co. This can be explained through chemical reactions that take place in parallel with electrodeposition. Chemical reactions are triggered only after application of current, which causes a large shift of the potential. The changes in catalytic properties of the cathode surface with deposition time result in a decline in the rate of the chemical reactions. The citrate ions in solution play an important role in creating a parallel chemical reduction, which only occurs at high negative potentials, generated by applying a high current density.

There are Ionic interactions in the electrolyte. A catalytic synergistic effect of nickel and perrhenate is observed. The process is controlled by mass transport and by the citric acid concentration. No evidence of perrhenate complexes with other components was found. There is an increased deformation of the perrhenate ions with increasing $[NiCit]^-$ /$[ReO_4^-]$. The induced co-deposition is a catalytic process, occurring on the surface by simultaneous reduction of ReO_4^- and $NiCit^-$, which influence each other by weak interaction.

Ultrathin (7 nm) Re-Ni layers with uniform thickness were electrolessly plated. Ni^{2+} is found necessary to obtain full surface coverage and thicker deposits. As-deposited Re-Ni films consist of both amorphous Ni-Re and $H_{0.57}ReO_3$ phases. The Re-content has a

maximal value at the percolation point. There are sequential reduction reactions, from ReO_4^- to metallic Re.

4.1.4 Atomic scale characterization

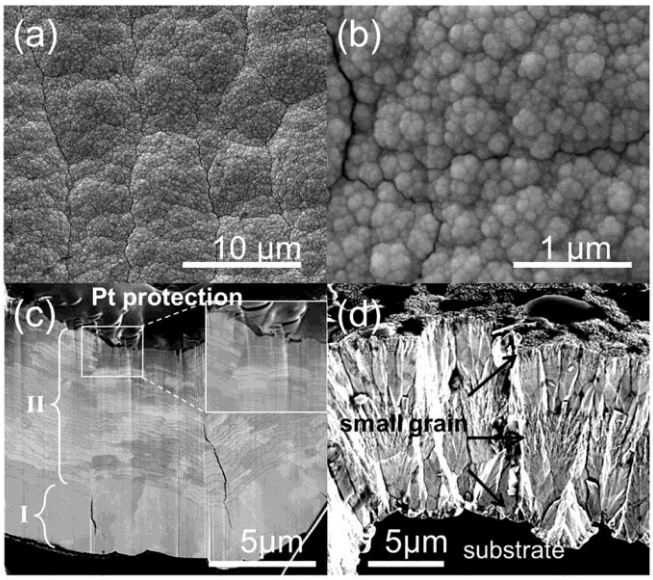

Figure 4.1. Re–Ni on 316L stainless steel substrate. (a, b) top surfaces, (c, d) cross-sections. (a, b) meso-scale colony structure. Volmer-Weber growth mechanism. (c) A bottom single-phase layer I, a top multilayer zone II. (d) Fracture surface revealing a columnar grain structure with several zones with different grain sizes across the coating. Layers with small grains are observed on the substrate and around the mid-thickness. The outer layer consists of a nodular structure. In between these layers, larger columnar grains dominate.

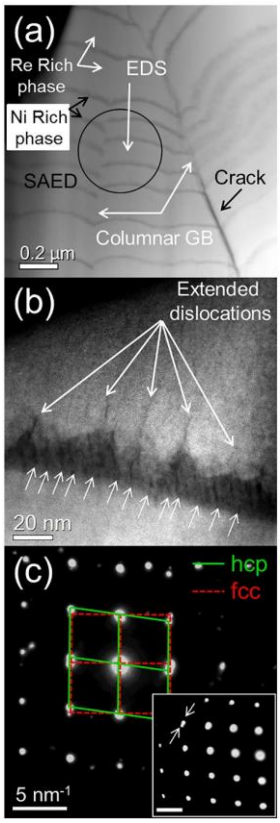

Figure 4.2. STEM-HAADF (high-angle annular dark-field) images and SAED patterns. (a) Alternating layers of a Re-rich phase (bright) and a Ni-rich phase (dark) within large columnar grains. A crack emanating along an inter-columnar GB, curvature of the Ni-rich layers, and a relative shift of these layers on both sides of an inter-columnar GB, are observed. (b) High-magnification image of the two interfaces between a Ni-rich layer (dark) and the adjacent Re-rich layers (bright). The upper interface in this image is rough and a high density of dislocations is apparent on this side. These two features are related to the epitaxial growth of the two phases and to stress relaxation at the interface, respectively. (c) The diffraction pattern from an hcp-Re-based phase exhibits an [1 -1 0 1] orientation (see inset). The diffraction pattern from a fcc-Re-based phase exhibits an [0 1 0] orientation.

4.1.5 Electrodeposition of Re-Ir-base alloys

The performance of Re at high-temperature in humid air is limited by the formation of rhenium heptoxide (Re_2O_7), which penetrates the grain boundaries and causes brittleness. Improvement of this was sought through the incorporation of iridium (Ir) into Re deposits. To this end, suitable plating baths for Re-Ir-Ni coatings were developed. These alloys were deposited from different aqueous solutions on copper substrates under galvanostatic conditions, in a three-electrode cell. The plating bath consisted of iridium tri-chloride, ammonium perrhenate and nickel sulfamate as the electroactive species, and citric acid as the complexing agent. The effects of bath composition and operating conditions on the FE, partial current densities, as well as on the thickness of the coatings and their composition were studied. The following conclusions were drawn:

- Re-Ir-Ni coatings as thick as 18 μm, with Re-content as high as 73 at.% and Ir-content as high as 37 at.%, were obtained, using different plating baths and operating conditions.
- The presence of citric acid in the bath exerted a considerable influence on the deposition process via the formation of various complexes with the metals.
- The ReO_4^- concentration seemed to have no significant effect on the partial current densities of Ir and Ni. This implies that the perrhenate anion does not take part in the rate-determining step for deposition of the alloy.
- As the concentration of Ni^{2+} in the solution was increased, coatings of high Re-content combined with a fairly high FE were obtained. The Ni^{2+} ions in the plating bath exhibit a distinct catalytic effect on the rate of Re deposition, but not vice versa.
- In contrast, increasing the Ni concentration in solution led to a significant decrease in the partial current density for deposition of Ir. We thus concluded that the deposition of Ni^{2+} and Ir^{3+} are competing reactions occurring in parallel. The concentration of Ir^{3+} in the bath does not seem to have a catalytic effect on the rate of deposition of Re.
- The effect of deposition time was studied. The mass gain showed a linear dependence on time up to 40 min, indicating a uniform rate of deposition corresponding to 14.1 μm/h. At longer times the rate of deposition declined as a result of the low volume-to-surface ratio of the bath employed in this study, and is not inherent to the system.
- A network of cracks was observed in all cases. Procedures for avoiding crack formation are a subject of further study in our laboratory.
- The ternary Re-Ir-Ni system showed a phase separation. A mixture of HCP Re-Ir-based phase and HCP Ni phase with nanometric crystallites were found in XRD measurements. To the best of our knowledge, this is the first systematic observation of the electrochemical formation of the HCP Re-Ir-based phase.

4.1.6 Electroless deposition of Re-Co and Re-Fe alloys

Electroless deposition may be preferable in many applications due to the combination of simplicity and low cost, low process temperature (<100°C), selective deposition and good via/trench filling, ability to coat very thin layers in the range of 10–100 nm on conductive and non-conductive substrates, either as a stand-alone coating or as a seed

layer for electroplating. The thin layer obtained by electroless plating is usually crack-free, and this can be useful particularly when electroplating the same metal may lead to formation of cracks.

One of the goals of this research was to develop electroless Re-base coatings on carbons, carbon-carbon composites, semiconducting and non-conducting surfaces. Pure Re cannot be deposited from electroless plating baths. Addition of other metal ions, such as Ni, Co, or Fe, is needed to establish induced codeposition of Re. At the end of Year 1 we presented our results on electroless deposition of Re-Ni alloys. During Year 2, high-quality films (10-100 nm thick) with high Re-content were obtained from Re-Co and Re-Fe baths. The kinetics of film deposition was strongly dependent on the iron-group metal concentration in the solution. Deposition on activated carbon was successful.

4.2 A Mechanistic Understanding of Re and Re-M Electrodeposition

4.2.1 Electrochemical Investigations

In order to get an insight into the possible molecular pathways leading to the Re-Ni electrodeposition from citrate baths, both experimental techniques and quantum-mechanical theoretical methods were used. The major findings from each of these approaches is presented. Molecular dynamics calculations were initiated using the Dmol3 module of the Materials Studio software. The semi-empirical Density Functional Theory-Perdue-Burke-Ernzerhof method (DFT-PBE) was used in combination with electrochemical techniques including potentiodynamic polarizations, galvanostatic methods and cyclic voltammetry.

Focus was placed on the understanding of the rhenium electrodeposition mechanism on a molecular level. To this scope, we addressed the following questions: What is the role of substrate? What is the role of the solvent? What is the structure of the double layer?

We learned that:

a) Citric acid strongly adsorbs on copper substrate and we proposed a model for such interaction mechanism.
b) Nickel ions form 1:1 Ni-citrate complex
c) A chemical “trigger” is required for the dissociation of such complexes that allows for the reduction of nickel.
d) Perrhenate ions readily reduce on copper, however the progress of the rhenium deposition is hindered by the catalytic effect that the metal possess toward the hydrogen evolution reaction.

Theoretical calculations have shown that:

a) The interaction between the copper and rhenium atoms is bridged by oxygen atoms and no evidence of direct interaction between copper and rhenium was found.
b) Under cathodic polarization, the copper surface strongly interacts with protons.
c) Protons are as likely to interact with perrhenate as with copper.

d) Nickel ions displace protons from the copper surface because they interact preferentially.

4.2.1.1 Interaction between the citric acid and copper electrode.

Copper exhibits an interesting electrochemical behavior under cathodic polarization in concentrated citrate solutions. The cyclic voltammogram of platinum and copper in de-oxygenated 343 mM citric acid at pH 5.0 (Fig. 2.1.1) shows that hydrogen evolution on copper is shifted cathodically by ca. 350 mV. This is consistent with the fact that the exchange current density (j_o) for proton reduction on copper is two orders of magnitude lower than on platinum. Additionally, while oxidation of hydrogen is detected on platinum during the reverse anodic scan, proton reduction on copper remains completely irreversible irrespective of the cathodic end-potential used in the cyclic voltammogram (CV) tests so that no hydrogen oxidation is observed.

Cathodic potentiodynamic polarization results in deoxygenated 343 mM citric acid as a function of pH are shown in Fig. 2.1.2. All curves displayed a current limited region followed by a region at more cathodic potentials where hydrogen evolution was under activation polarization control. The current density in the limited region was pH-dependent. The largest current was measured at pH 2.0 and the lowest at pH 6.5. These limited currents are attributed to under-potential reduction of protons from adsorbed citric acid molecules where the acidic protons of citric acid are pointed towards the negatively polarized copper surface. As indicated by the three pK values of 3.09, 4.75 and 5.41 for citric acid, at pH 2.0 (90% H_3Cit, 10% H_2Cit^-) up to three acidic protons are carried by each citric acid molecule, while at pH 6.5 (87% Cit^{3-}, 13%

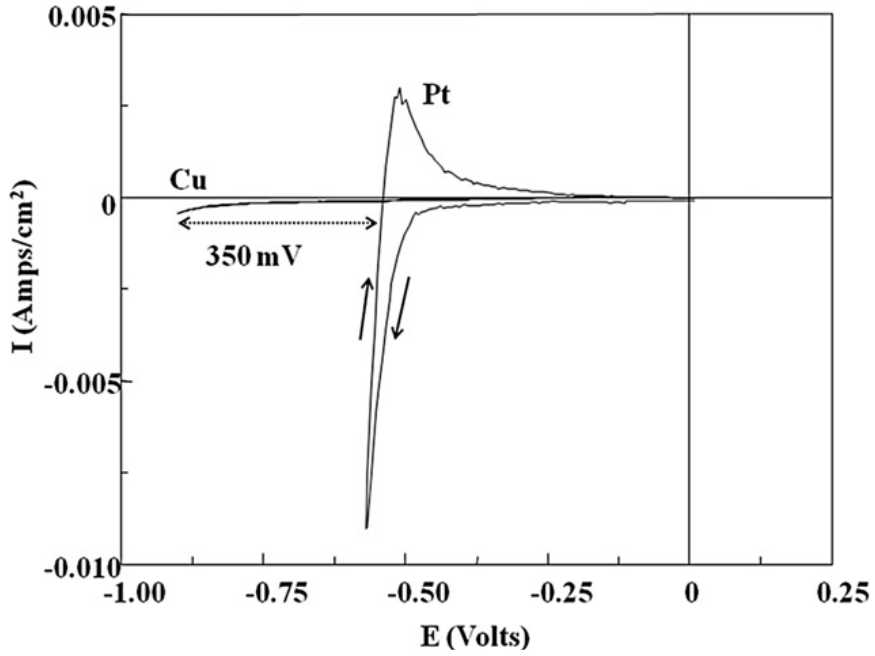

Figure 2.1.1. Comparison between the cyclic voltammograms of copper and platinum immersed in 343 mM citric acid at pH 5.0.

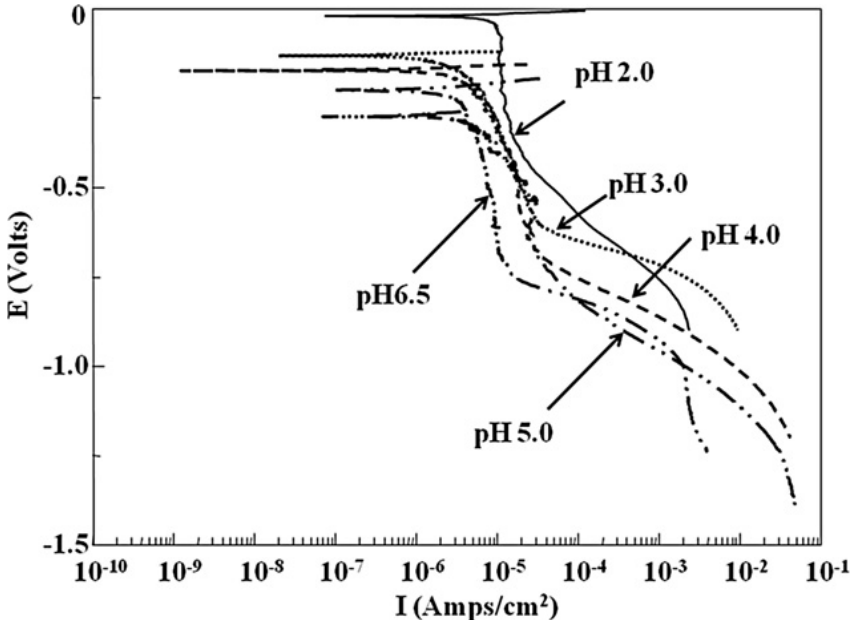

Figure 2.1.2. Comparison between the cathodic potentiodynamic polarization curves of copper 343 mM citric acid as a function of pH.

$HCit^{2-}$) only one proton can be carried by each citric acid molecule. Therefore, at pH 2.0 the current due to the underpotential reduction of such protons is expected to be signify-cantly larger than at pH 6.5.

The interaction between citric acid and copper was corroborated by double layer capacitance (C_{dl}) measurements obtained from electrochemical impedance spectro-scopy (EIS). Since citric acid can only carry one proton at pH 6.5, the interaction between copper and the organic molecule is proposed to be via onsite adsorption where the organic molecule approaches the copper electrode in an end-on configuration. Consequently, the thickness of the double layer is anticipated to be determined by the length of the citric acid molecule. At pH 2.0, citric acid is fully protonated and the ad-sorption on copper is assumed to be by all three carboxylic acid protons. Thus, the citric acid molecule approaches the electrode in a lengthwise configuration parallel to the sur-face yielding a double layer thickness that is reduced relative to the one-site adsorption predicted at pH 6.5. As a result, the double layer capacitance at pH 2.0 is expected to be significantly larger than at pH 6.5 due to the inverse relationship between capaci-tance and space charge separation. This outcome was experimentally verified through EIS. Furthermore, the interfacial impedance of copper immersed in citric acid signify-cantly increased with increasing pH as illustrated in Fig. 2.1.3. This is consistent with the decrease in the number of protons carried by the adsorbed citric acid at higher pHs, which decreases the ability for charge transfer and increases the interfacial impedance.

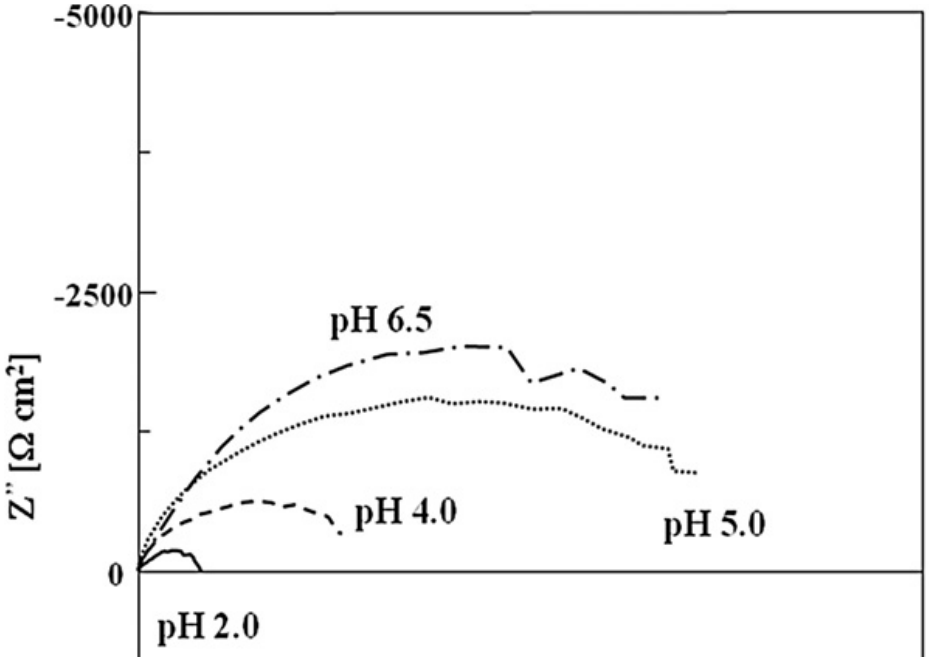

Figure 2.1.3. Nyquist plot of copper in 343 mM citric acid as a function of pH. Spectra collected at open circuit potential.

Interestingly, while the presence of citric acid in the double layer facilitates the reduction of protons, it also inhibits the electron transfer involving foreign redox systems. This can be seen by comparing the voltammetric response of $[Fe(CN)_6]^{3-}/[Fe(CN)_6]^{2-}$ on copper immersed in citric acid and in sodium sulfate at the same pH (Fig. 2.1.4). It is apparent from Figure 2.1.4 that the strong reduction and oxidation reactions observed in sodium sulfate are dramatically inhibited in citric acid. Based on these results, a critical advantage that results from the use of concentrated citric acid as an electrolyte for electroplating copper substrates is the increase in the Faradic impedance associated with the reduction of the depositing species. An increased interfacial impedance along with the inherent increase in electrolyte conductivity will produce a favorable bath throwing power.

Figure 2.1.4. Voltammetric response of 2.4 mM $[K_3Fe(CN)_6]$ at copper electrode immersed in 343 mM citric acid at pH 5.0 and 1 M sodium sulfate at the same pH.

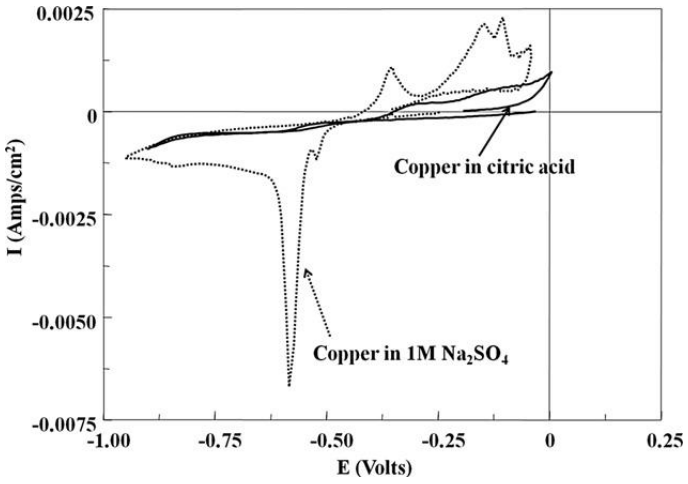

4.2.1.2 The interaction between citric acid, Ni(II) and ReO_4^-

UV–vis absorption spectroscopy is a powerful technique that can determine whether transition metal cations form complexes with electron-donor molecules, i.e. ligands. This technique relies on the fact that the energy of the central cation d-orbitals changes when chemically coordinated by ligands. Since the energy difference between the various d-orbital falls within the UV–vis range of the electromagnetic spectrum, changes in color and/or UV absorption characteristics are often indicative of complex formation. Figure 2.1.5 shows the UV–vis absorption spectra of nickel sulfamate and citric acid at pH 5.0 as a function of Ni(II)/citric acid molar fraction. It is apparent that aqueous nickel sulfamate solutions display three major absorption peaks at 380, 620 and 740 nm which

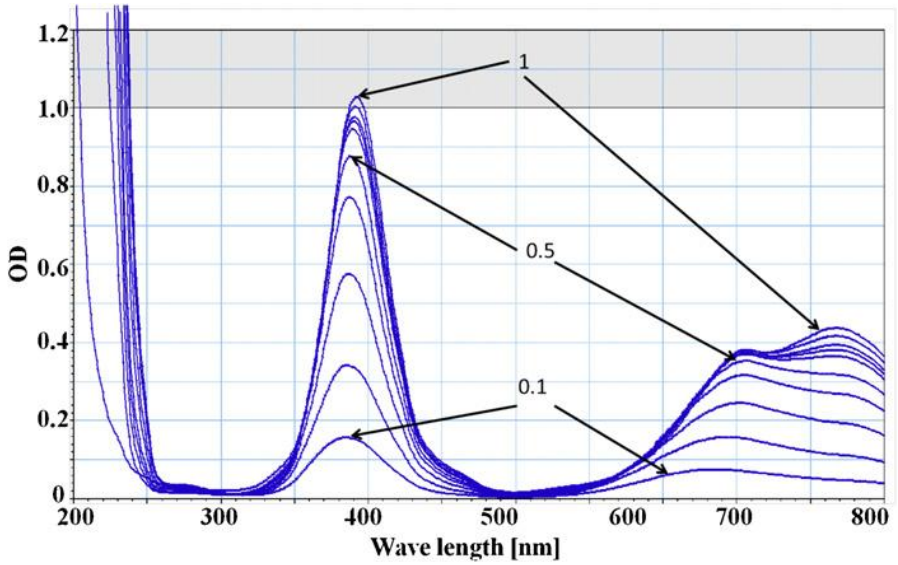

Figure 2.1.5. UV–Vis spectra of nickel sulfamate and citric acid at pH 5.0 with Ni/citrate molar fraction ranging from 1 to 0.1 in 0.1 increments.

are typical of the nickel esa-aquo complex $[Ni(H_2O)_6]^{2+}$. These absorption maxima are shifted to higher energy when citric acid is added to the nickel sulfamate solutions. Such absorption energy shifts are due to the crystal field strength of Ni(II) which becomes progressively higher when citric acid molecules substitute for water molecules in the nickel esa-aquo complex. The formation of Ni–citrate complexes is clearly indicated by the fact that the absorbance due to $[Ni(H2O)_6]^{2+}$ is not proportional to the Ni(II) ion concentration. Figure 2.1.6 shows the absorbance variation of nickel sulfamate solutions and Ni–citric acid mixtures as a function of Ni/citric acid molar fraction. The difference between the two curves shown in Fig. 2.1.6 corresponds to the absorbance

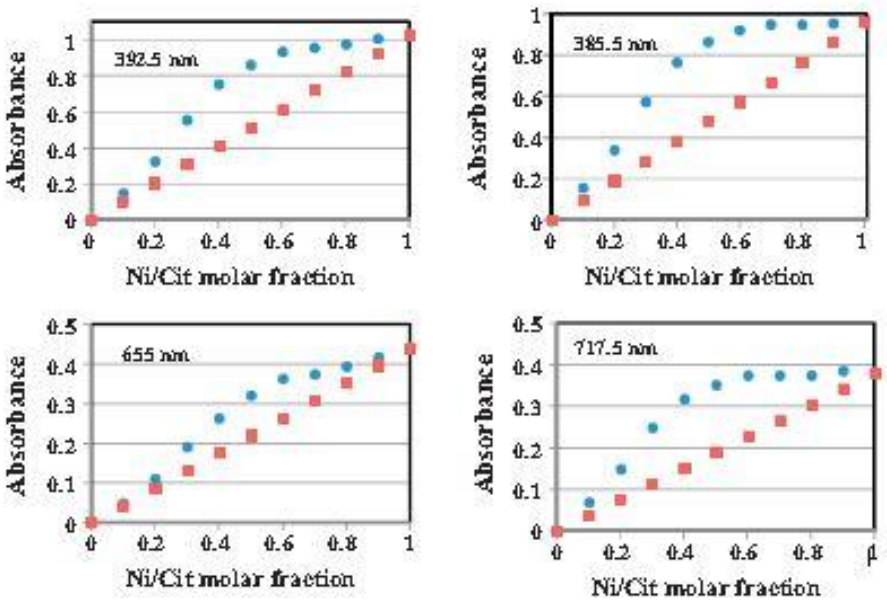

Figure 2.1.6. Absorbance of nickel sulfamate (squares) and nickel + Ni–citrate (circles) at different Ni/citrate molar fractions and at different frequencies.

of the Ni–citric acid complexes which is shown in Fig. 2.1.7. Since the maximum absorbance of Ni–citrate complexes is reached at a Ni–citrate molar fraction of 0.5, we propose that Ni(II) forms 1:1 complexes with citric acid at pH 5.0. At least three 1:1 complexes between Ni(II) and citric acid are known: $[NiH_2Cit]^+$, [NiHCit] and $[NiCit]^-$. The negative logarithm of their formation equilibrium constants (pK_f) are ca. 1.5, 3.4 and 5.5 respec-tively. At alkaline pH, the 1:2 complex $[Ni(Cit)_2]^{4-}$ is known and its pK_f is 2.4. Therefore, at pH 5.0, the most stable 1:1 complex $[NiCit]^-$ initially predominates, which allows the electrical double layer to enrich in Ni(II) species. With progressive hydrogen evolution, the interfacial pH becomes more alkaline, and the 1:2 complex becomes the predomi-nant species. However, since the stability constant of the 1:2 complex is not large enough to sustain the high concentration of the 1:1 species, the excess 1:1 complex dissociates releasing Ni(II) ions which can then promptly reduce.

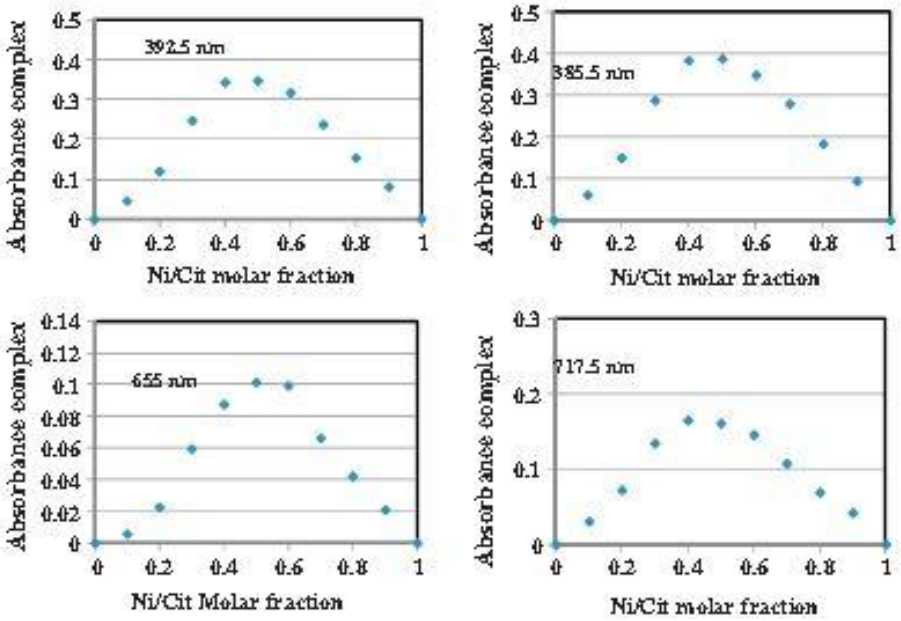

Figure 2.1.7. A plot of the difference between the absorbance of nickel sulfamate (squares) and nickel + Ni–citrate (circles) data in Figure 2.1.6.

Ammonium perrhenate and citric acid each intensely absorb UV radiation at pH 5.0. However when these two compounds were mixed together in any molar ratio, their respective absorption characteristics did not change. This finding was consistent with past unsuccessful attempts to characterize ReO_4–citric acid complexes by UV–vis absorption spectroscopy. Although it is known that anions can be coordinated by negatively charged organic molecules with the electrostatic repulsion offset by intermolecular rearrangements, entropic gains, hydrogen bonds and Van der Waals-type interactions, our UV–vis absorption tests indicate that the ReO_4^- anions is unlikely to chemically bind to dissociated citric acid. Therefore, it is assumed here that even in the presence of a molar excess of citrate ions, the ReO_4^- ion remains hydrated or coordinated by ammonium cations. It is interesting to point out that the results discussed so far have shown that the use of concentrated citric acid for the electro-deposition of Re–Ni alloys on copper substrates has two significant advantages. First, the adsorption of citric acid on the copper substrate increases the interfacial impedance associated with the electron transfer of metal ion reduction. Second, by complexing nickel ions, citric acid causes a dramatic decrease in the exchange current density of nickel reduction, which potentially increases the partial current density of Re electro-reduction as well as the throwing power of the plating bath.

4.2.1.3 Mechanism of Ni(II) reduction

The CV of copper immersed in 1 M sodium sulfate with and without nickel sulfamate, clearly shows the current waves due to nickel reduction and oxidation (Fig. 2.1.8). The large separation between the anodic and cathodic peaks is due to the slow rate of electron transfer typical of irreversible systems, while the low ratio between the anodic and cathodic current peaks is due to the fact that the oxidation of metallic nickel is

limited by nickel passivation. Additionally, as it is apparent from the dramatic increase in the current due to the hydrogen evolution reaction, proton reduction preferentially occurs on the electroformed metallic nickel rather than on the copper substrate.

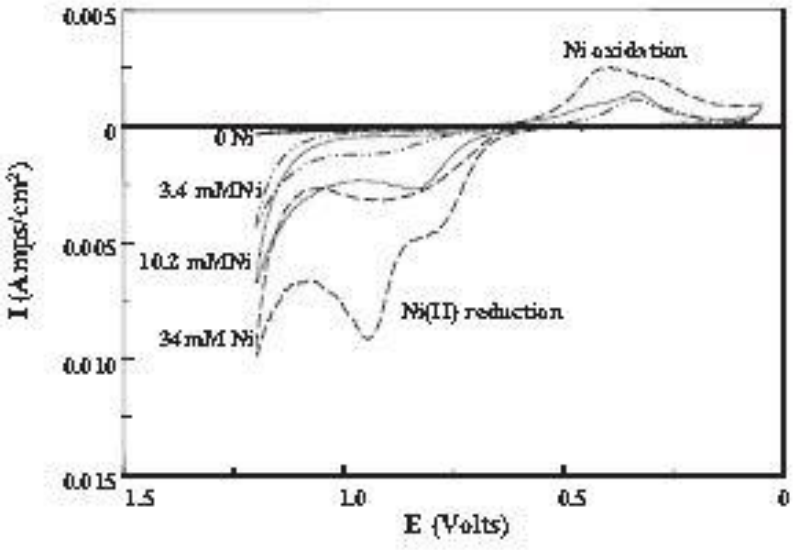

Figure 2.1.8. Cyclic voltammograms of copper in 1 M sodium sulfate containing increasing amounts of nickel sulfamate

When experiments were conducted in citric acid (Fig. 2.1.9), the current wave for Ni(II) reduction was no longer distinguishable because it was convoluted with the current due to hydrogen evolution. Interestingly, when nickel was added to citric acid, the potential

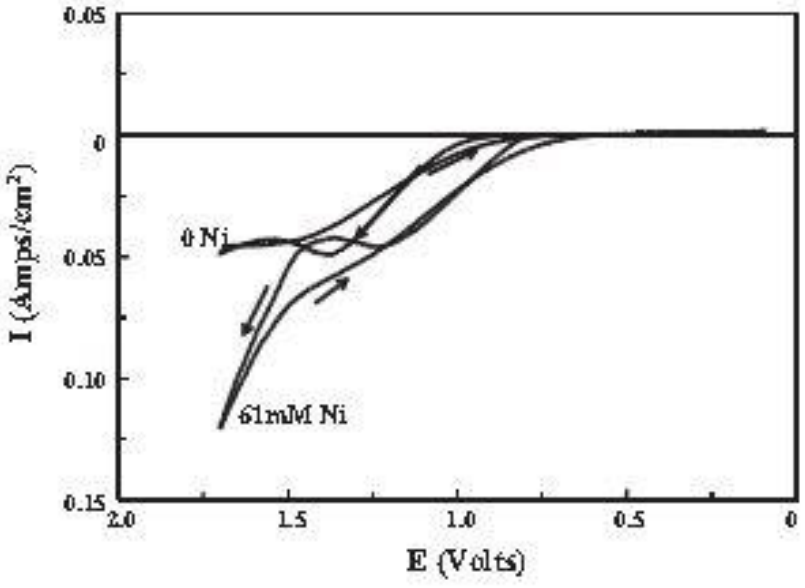

Figure 2.1.9. Effect of nickel sulfamate on the cyclic voltammograms of copper in 343 mM citric acid at pH 5.0.

at which the hydrogen evolution reaction occurred was significantly shifted anodically indicating that nickel ions catalyzed the proton reduction (Fig. 2.1.9). This effect is also confirmed by the loop generated by the higher cathodic current recorded during the reverse potential scan. The small current loop observed in citric acid was instead due to

citric acid desorption which allowed more proton discharge. CVs conducted at progressively increasing cathodic end-potentials showed that it was necessary to polarize the copper electrode below −1.3 V vs Ag/AgCl to detect the current due to nickel oxidation.

Such potential shifts were initially explained by the decrease in the activity of the Ni(II) ions due to complex formation with citrate species. However, given the fact that nickel reduction on copper is highly irreversible (see Fig. 2.1.8), conducting experiments at a lower scan rate was essential to verify if indeed nickel reduction was controlled by thermodynamic driving forces due to complex formation. Cathodic potentiodynamic polarization experiments conducted in citric acid at pH 5.0 with increasing concentration of nickel sulfamate are reported in Fig. 2.1.10. The increase in nickel ions concentration causes: (1) an increase in the current due to under-potential proton reduction, and (2) a ca.130 mV anodic shift of the potential at which proton reduction is controlled by activation polarization. Qualitatively, the effect of nickel ions was similar to that of adding an acid to the solution. This finding is supported by potentiometric titration experiments in citric acid with and without nickel ions. Such experiments have demonstrated that nickel ions increase the citric acid buffer capacity by: (1) making the alcoholic proton of the organic molecules acidic, and (2) generating additional acidic protons from the water molecules directly coordinated to the nickel cation. Since the

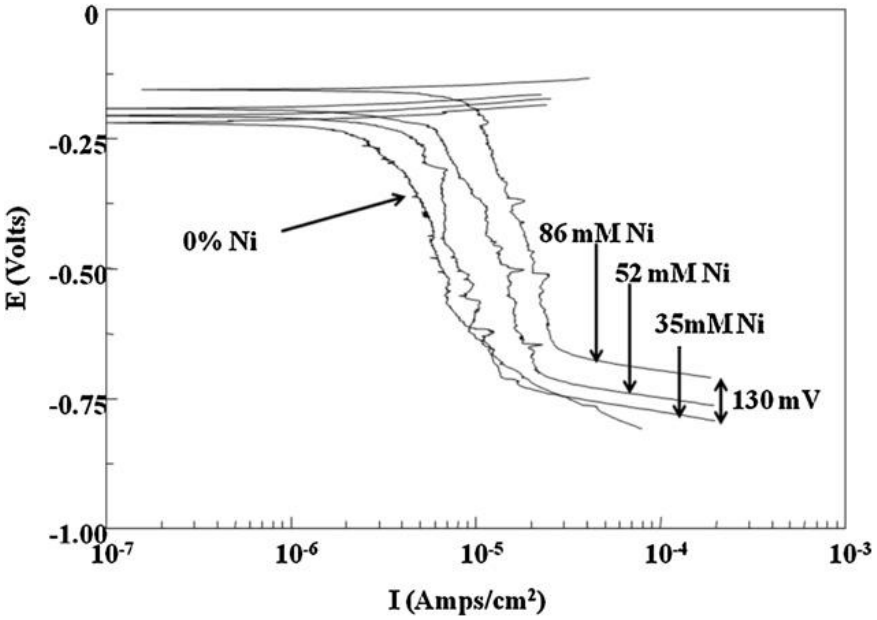

Figure 2.1.10. Effect of nickel sulfamate on the cathodic potentiodynamic polarization curves of copper in 343 mM citric acid at pH 5.0.

copper rod was covered by a gray layer of metallic nickel at the end of each potentiodynamic scan shown in Fig. 2.1.10, it was apparent that the increase in nickel ion concentration also caused the reduction potential of nickel to shift anodically by ca. 130 mV. Additionally, the results of the polarization experiments shown in Fig. 2.1.10 demonstrated that nickel reduction could occur at potentials significantly more anodic than −1

V in contrast to what the CV tests indicated. Therefore, we concluded that the reduction of nickel is kinetically dependent on the reduction of protons rather than controlled by the activity of Ni(II) in solution through the Nernst equation. In fact, given the large molar excess of citric acid, as well as the high values of the pK_f of the Ni(II)–citrate complexes, the activity of free nickel ions is not expected to change as long as citric acid remains in molar excess.

The effect of nickel ions concentration on the cathodic potentiodynamic plots shown in Fig. 2.1.10 can be explained by having a closer look at the structure of the nickel complexes that form in aqueous citric acid. It is known that octahedral coordination is one of the two most common geometries of Ni(II) complexes. Therefore, the 1:1 Ni(II)–citrate complexes are shown in Fig. 2.1.11a and b as coordinated by up to 5 water mole-cules and 1 citrate molecule. In representing the octahedral compounds, it was assumed that only the oxygen atoms of the carboxylic acid groups are involved in the complex formation with Ni(II). However, it is known that the oxygen atom of the alcoholic group may also participate in coordinating the central cation. The positively charged complex (Fig. 2.1.11a) is deemed to be more likely to migrate towards the copper surface when the copper

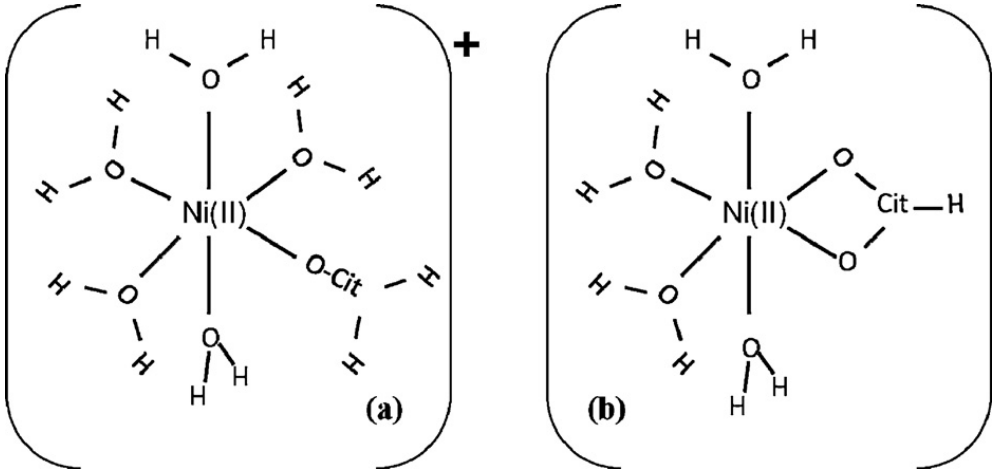

Figure 2.1.11. (a) Octahedral 1:1 $[Ni(H_2O)_5(H_2Cit)]^+$ and (b) $[Ni(H_2O)_4(HCit)]$ complexes.

electrode is polarized cathodically. The significant increase in the underpotential proton reduction observed when nickel was added to citric acid is attributed to the fact that each nickel ion specifically adsorbed onto copper carries with it a large number of acidic protons from the coordinating water molecules and the coordinating citrate ligand. However, nickel ions cannot reduce until they are dissociated from the citrate complex. This dissociation is thought to be triggered by the alkalinization of the interface due to the hydrogen evolution reaction. In fact, the increase in the electrode interfacial pH causes the formation of the 1:2 complex $[Ni(Cit)_2]^{4-}$, which has a dissociation constant that is several orders of magnitude larger than the 1:1 $[NiCit]^-$ complex existing at pH

5.0. Since the concentration of $Ni[Cit]^-$ is far greater than what is permitted by the pK_f of the 1:2 complex, the excess $Ni[Cit]^-$ dissociates releasing free Ni(II) ions which promptly reduce. This mechanism can explain the experimental results illustrated in Fig. 2.1.10. The increase in the analytical concentration of nickel ions produces a corresponding increase in the concentration of proton-carrying nickel–citrate complexes that decrease the interfacial pH and allows the hydrogen evolution reaction to start at less cathodic potentials. At the same time, as soon as the hydrogen evolution reaction causes the interfacial pH to increase sufficiently, the nickel–citrate complexes start to dissociate releasing free nickel ions, which explains why the reduction of nickel is always confluent with the hydrogen evolution reaction.

4.2.1.4 Reduction mechanism of NH_4ReO_4

A strong catalytic effect of citric acid on the electroreduction of perrhenate was proposed by Vajo et al. who reported that the polarografic reduction half-wave potential of ReO_4^- in 1 M KCl was shifted anodically by over 500 mV in the presence of citric acid. They attributed this effect to the formation of the 1:1 complex $[ReO_4H_2Cit]^{2-}$ that they could not however isolate or characterize by UV–Vis spectroscopy. In order to confirm the catalytic effect of citric acid on the reduction of perrhenate on copper substrates, we studied the cyclic voltammograms of copper in 1 M sodium sulfate and 343 mM citric acid at the same pH with and without ammonium perrhenate. As shown in Fig. 2.1.12, in 1 M Na_2SO_4, perrhenate ions reduce on copper around −1 V right before the reduction o

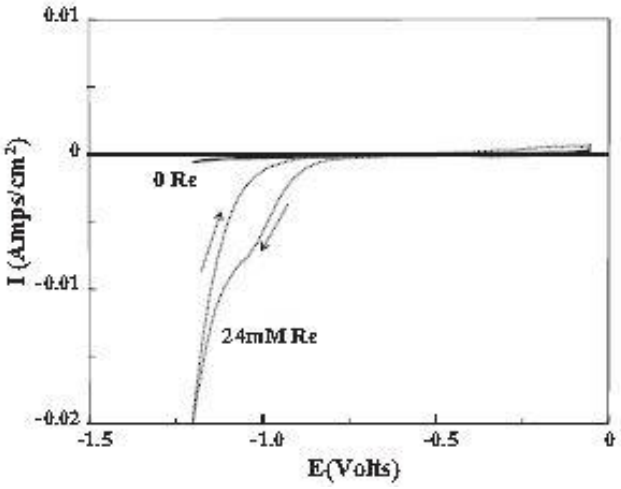

Figure 2.1.12. Effect of 24 mM NH_4ReO_4 on the cyclic voltammogram of copper in 1 M Na_2SO_4 at pH 6.0.

of water. If the electrode is held at −1 V, it rapidly be-comes coated by a silvery rhenium film. Fig. 2.1.13 shows the CV of copper in citric acid with and without ammonium perrhenate. The CV of citric acid distinctly shows the reduction wave of the protons carried by the citric acid where the maximum current density is proportional to the bulk concentration of the organic acid. In the presence of perrhenate ions, the overall reduction wave is shifted anodically and the diffusion limiting current density increases by about 6 mA/cm^2. The anodic shift of the cathodic wave is attributed to the reduction

of perrhenate ions which reduce preferentially compared to protons even in the presence of strongly adsorbed citric acid.

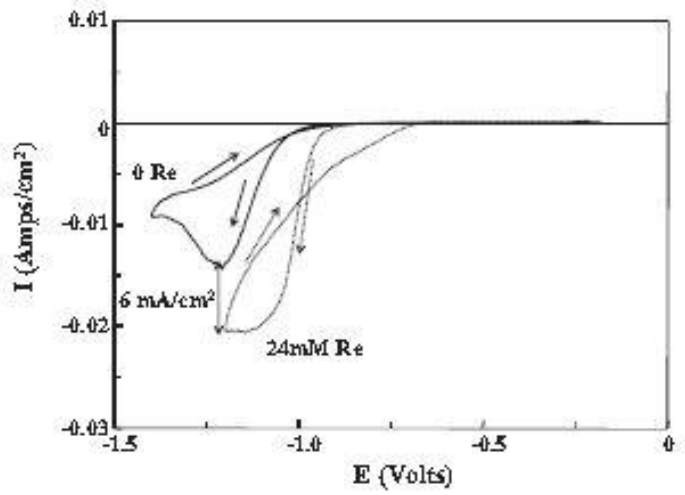

Figure 2.1.13. Effect of 24 mM NH_4ReO_4 on the CV of copper in 343 mM citric acid at pH 6.0.

Given the strong adsorption properties of N-containing organic molecules on copper, it is likely that ammonium ions compete with citric acid for adsorption sites on the copper surface. These cations electrostatically attract the perrhenate anions allowing them to reach the double layer where they reduce to metallic rhenium. However, as soon as rhenium atoms are deposited, they provide a substrate where the hydrogen evolution reaction can occur at a lower overvoltage to become the predominant cathodic process. As a matter of fact, the increase in the diffusion limiting current density caused by the perrhenate ions is almost identical to the intensity of the current wave due to the perrhenate reduction observed in sodium sulfate (Fig. 2.1.12). Moreover, the current loop observed in citric acid containing ammonium perrhenate is a clear indication of the catalytic effect of rhenium toward the hydrogen evolution reaction. Such current loop is not observed in sodium sulfate because this solution does not act as a buffer and the interfacial pH becomes strongly alkaline during the forward cathodic potential scan. The comparison between Figs. 2.1.12 and 2.1.13 shows that the reduction of perrhenate ions in sodium sulfate and in citric acid occurs at the same potential, that is, around −1 V. Therefore, our data indicate that citric acid does not catalyze the reduction of perrhenate ions. On the other hand, the data presented here demonstrate that: (1) the reduction of perrhenate ions is not affected by the electrolyte, and (2) it occurs preferentially compared to the hydrogen evolution reaction. However, once rhenium species are reduced they catalyze the protons discharge which becomes the predominant electrode process. This is known to be the intrinsic reason why the deposition of pure rhenium from aqueous solutions occurs with very low Faradic efficiency. Therefore, one way to increase the Faradic efficiency of rhenium electroreduction from aqueous electrolytes is to introduce another element, for example nickel, which when deposited creates a substrate that preferentially allows rhenium reduction rather than proton discharge.

4.2.1.5 Proposed mechanism for Re–Ni electrodeposition

The results presented here suggest that under intense cathodic polarization of copper in a nickel sulfamate/ammonium perrhenate/citric acid bath, the following reactions occur:

$$[Ni(H_2O)_5(H_2Cit)]^{+} + 2e^{-} = [Ni(H_2O)_3Cit]^{-} + H_2 + 2H_2O \quad (1a)$$
$$2Hcit^{2-} + 2e^{-} = H_2 + 2Cit^{3-} \quad (1b)$$
$$H_2cit^{-} + 2e^{-} = H_2 + 2Cit^{3-} \quad (1c)$$

The progressive alkalinization of the interface caused by reactions (1a), (1b) and (1c) allows the formation of the 1:2 complex shown in reaction (2)

$$[Ni(H_2O)_3Cit]^{-} + Cit^{3-} = [Ni(Cit)_2]^{4-} + 3H_2O \quad (2)$$

The formation constant of the 1:2 Ni–citrate complex cannot sustain the high concentration of the 1:1 complex. Therefore, following reaction (1a), the $[NiCit]^{-}$ complex dissociates releasing Ni(II), which promptly reduces to metallic nickel.

$$Ni^{2+} + 2e- = Ni \quad (3)$$

In the meantime because of electrostatic repulsion, the negatively charged citrate ion leaves the electrode interface and migrates away from the double layer where it can get protonated again. The reduction of the perrhenate ion takes place in parallel with reactions (1a), (1b), (1c), (2) and (3),

$$NH_4ReO_4 + 7e^{-} + 4H_2O = Re + NH_4 + + 8OH^{-} \quad (4)$$

The formation of metallic rhenium immediately increases the rate of the hydrogen evolution reaction, however, the parallel nickel reduction and the resulting repulsion between the negatively polarized electrode and the citrate ions creates room for additional NH_4ReO_4 to adsorb onto the electrode surface allowing more rhenium to deposit.

4.2.2 Mechanistic understanding based on DFT calculations

It is hypothesized that the observed synergy must result from the interaction between Ni^{2+}, perrhenate and citrate ions. The concept of perrhenate and citrate interaction with formation of a reversible electroactive perrhenate/citrate complex $(H_2CitReO_4)^{2-}$ was used to explain a dependence of the limiting current Re(VII) reduction on citrate and $(ReO_4)^{-}$ concentration at pH 3.12 and 3.30, respectively. However, no proof for such a complex was provided. While the existence of Ni^{2+} coordination compounds with citrate species is well documented using UV visible spectroscopy, similar approaches have not shown complexes between perrhenate ions and citrate species.

The aim of the present work is to provide theoretical evidence of the existence of chemical interactions between ReO_4^{-}, Ni^{2+} and citrate ions. Quantum chemical calculations may provide insight into the chemical interactions of perrhenate, ReO_4^{-}, with citric acid, H3Cit, citrate ion, H_2Cit^{-}, and Ni-citrate complexes: NiH_3Cit^{2+}, NiH_2Cit^{+} and $Ni(H_2Cit)_2$. In this work we use Density Functional Theory (DFT) to investigate the

structure and electrochemical properties of these species. Among the DFT functionals, B3LYP has been widely used to investigate a wide number of chemical systems. Here we use this DFT functional in combination with compact effective potential (CEP) basis sets to optimize the geometry of different ReO_4-citrate and ReO_4-Ni-citrate systems and to calculate their respective single-point energy. The obtained energy values are then incorporated into a thermodynamic cycle to determine the standard Gibbs free energy (ΔG), enthalpy (ΔH), entropy (ΔS) and reduction potentials (E).

Computational Method

a. Structures Geometries

Perrhenate and Perrhenate-Citrate Adducts: The geometry of perrhenate (ReO_4^-) and the ReO_4^-/citrate adducts was optimized at the B3LYP/CEP-121G theory level. The structures of ReO_4^- and the ReO_4^-/citrate adducts are shown in Fig 1. Citric acid (H_3Cit) and the protonated ions H_2Cit^- and $HCit^{2-}$ are the most abundant at pH below 5. Three different interactions of ReO_4^- with H_3Cit were examined. Four different interactions of ReO_4^- with H_2Cit^- were examined. Two of these structures were based on the $[ReO_4H_2Cit]^{2-}$ complex proposed by Vajo et al.

Geometry optimization of the interaction of ReO_4^- with $HCit^{2-}$ resulted in a high repulsion with a distance of approximately 63Å between the Re atom in perrhenate and the C atom of the carboxylate group in the citrate ion. For this reason, we did not include the ReO_4^-/$HCit^{2-}$ adduct in this work.

Nickel (II)-Citrate Complexes: The Ni^{2+}-citrate complexes considered in this work are NiH_3Cit^{2+}, NiH_2Cit^+ and $Ni(H_2Cit)_2$. The geometry of each complex was optimized at the B3LYP/CEP-121G theory level.

ReO_4^-/Ni^{2+}-Citrate Adducts: Different interactions of ReO_4^- with NiH_3Cit^{2+}, NiH_2Cit^+ and $Ni(H_2Cit)_2$ were examined. The geometry of each adduct was optimized at the B3LYP/CEP-121G level of theory.

b. Frequency Calculations

A frequency calculation was performed at 298.15 K and 1.0 atm with a scale factor of 0.96 to obtain the zero-point energy correction and thermal correction to the enthalpy and free energy.

c. Enthalpy and Free Energy

The interactions of ReO_4^- with citrate and the Ni^{2+}-citrate complexes are described by the following equations:

$$ReO_4^- + H_3Cit = ReO_4^-/H_3Cit \quad (1)$$

$$ReO_4^- + H_2Cit^- = ReO_4^-/H_2Cit^- \quad (2)$$

$$ReO_4^- + Ni^{2+}\text{-Citrate (C, D or E)} = ReO_4^-/Ni^{2+}\text{-Citrate (C, D or E)} \quad (3)$$

The gas-phase enthalpy of equations 1 – 3 was calculated using the following equation:

$$\Delta H = \Delta E + \Delta H_{corr} \quad (4)$$

where ΔE is the difference in the electronic energy between product and reactant, and ΔH is the difference in the thermal correction to the enthalpy of product and reactant. The electronic energy (E) of each structure was calculated performing a single point energy at the B3LYP/CEP-121G level of theory.

Gas-phase free energy was determined by the expression:

$$\Delta G_{gas}(1atm) = \Delta E + \Delta G_{corr} \quad (5)$$

The correction to the free energy was calculated by frequency calculations at 1.0 atm of pressure. Conversion of the free energy at 1 mol/L conditions is calculated by:

$$\Delta G_{gas}(1mol/L) = \Delta G_{gas}(1atm) + RT\ln(24.46) \quad (6)$$

Change in entropy, ΔS was calculated at T = 298.15 K by

$$\Delta G_{gas}(1mol/L) = \Delta H - T\Delta S \quad (7)$$

In equation 7, $\Delta G_{gas}(1mol/L)$ is the free energy obtained from equation 6. The change in enthalpy, ΔH, was calculated from equation 4, and *T* is the temperature. The free energy of equations 1 – 3, in aqueous solution, was calculated from the thermodynamic cycle shown below.

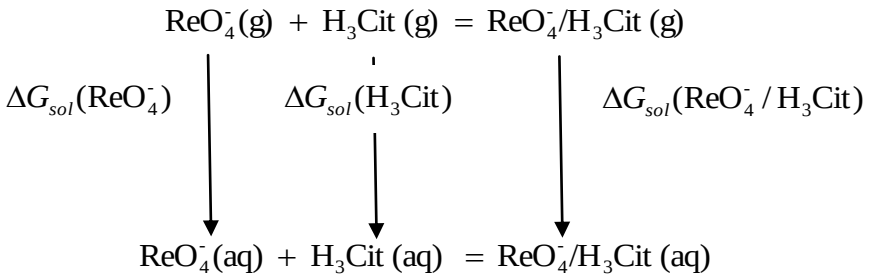

The aqueous free energy at 298.15 K was calculated from equation 8.

$$\Delta G_{aq}^{298.15K} = \Delta G_{gas}(1mol/L) + \Delta\Delta G_{sol} \quad (8)$$

In this equation, $\Delta G_{gas}(1mol/L)$ is the gas-phase free energy at 1 mol/L conditions calculated from equation (6) and $\Delta\Delta G_{sol}$ is the difference in solvation energies between product ($\Delta G_{sol}(\text{product})$) and reactant ($\Delta G_{sol}(\text{reactant})$). The solvation energies of ReO_4^- and its adducts were calculated using the self-consistent reaction field conductor-like polarized continuum model (SCRF-CPCM) at B3LYP/CEP-121G theory level.

d. Reduction Potentials

The reduction of ReO_4^- in acidic solution is described by the following chemical equation:

$$7e^- + 8H^+ + ReO_4^- = Re + 4H_2O \quad (9)$$

The total free energy of the reduction of ReO_4^- in the different adducts are determined by adding the inverse of the chemical equations 1, 2 or 3 and chemical equation 9.

$$\begin{array}{lll} ReO_4^-/H_3Cit = ReO_4^- + H_3Cit & & -\Delta G_{aq}^{298.15K} \\ 7e^- + 8H^+ + ReO_4^- = Re + 4H_2O & & \Delta G_{Re^{7+}/Re} \\ \hline 7e^- + 8H^+ + ReO_4^-/HCit = Re + 4H_2O + H_3Cit & & \end{array}$$

$$\Delta G_{Re^{7+}-Cit/Re} = \Delta G_{Re^{7+}/Re} - \Delta G_{aq}^{298.15K} \quad (10)$$

The $\Delta G_{Re^{7+}/Re}$ and $\Delta G_{aq}^{298.15K}$ terms are calculated using the thermodynamic cycle described above.

The reduction potential (ε) versus the standard hydrogen electrode (SHE) are determined based on the redox process:

$$\begin{array}{lll} 7e^- + 8H^+ + ReO_4^-/H_3Cit = Re + 4H_2O + H_3Cit & & \Delta G_{Re^{7+}\text{-}Cit/Re} \\ 7\times(\tfrac{1}{2}H_2 = H^+ + e^-) & & 7\Delta G_{H_2/H^+} \\ \hline \tfrac{7}{2}H_2 + H^+ + ReO_4^-/H_3Cit = Re + 4H_2O + H_3Cit & & \end{array}$$

$$\Delta G_{vsSHE} = \Delta G_{Re^{7+}\text{-}Cit/Re} + 7\Delta G_{H_2/H^+} = -nF\varepsilon \quad (11)$$

In equation 10, *n* is the total of electrons involved in the redox process (7 electrons) and *F* is the Faraday number 96,485 C mol-1 (23.061 kcal/Vmol). The reduction potential of the SHE used in these calculations was 4.42 V. All calculations were performed using the computer code Gaussian 09W.

Based on the standard Gibbs free energy (ΔG), enthalpy (ΔH), entropy (ΔS) and reduction potential (E) calculations, our thermodynamic investigation of the interactions of ReO_4^- with citrate and a Ni-citrate complexes show:

1. Perrhenate ions are not likely to form any kind of interaction with citrate species.
2. Perrhenate ions are most likely to form interactions with Ni-citrate complexes.
3. Modification in the reduction potential of Re^{7+} and Ni^{2+} depends on the citrate specie structure implying that pH influences in the reduction process. Reduction of Re^{7+} and Ni^{2+} can be improved at higher pH consistent with experimental results indicating that Faradaic efficiency in electrodeposition increases at higher pH.

5.0 DEPOSITION OF Re-M FILMS ONTO SUBSTRATES RELEVANT TO DoD

Most of the deposition research performed in this study was conducted on copper substrates. Copper is a metal whose native oxide film is easily reduced. It can be cleaned in nitric acid so that it presents essentially a bare metal substrate to an electrodeposition process, particularly when polarized cathodically. This allows metal-to-metal bonding occur more easily between the deposited film and the substrate, thus facilitating good bonding between the coating and substrate. Similar phenomenon would occur between a silver substrate and electrodeposited metal coating. Historically, this is why most successful electroplating process used copper, brass (copper-zinc alloy), and silver as substrates. Scientifically, these investigators attribute this effect to the heat of formation (H_f) of the substrate metal oxide.

When the substrate metal or alloy has an oxide that has a high H_f, *e.g*., nickel-based alloys, the ability to successfully electrodeposit a metal coating is much more difficult and forms the basis of the thousands of known and proprietary recipes for substrate preparation and electrodeposition methods. It is likely that any method that is successful on high temperature alloy substrates, wil use either a cleaning process that roughens the substrate and/or an electroless strike layer. The strike layer is a seed layer typically of another material, that lays down through an electroless deposition process. This does not guarantee that the electrodeposited coating will adhere well to the substrate.

We attempted to electrodeposit Re-Ni coatings on Inconnel 625, a Ni-based, high temperature alloy using both a Wood's strike layer (electroless Ni) and an elaborate cleaning method specified for this alloy. Neither of these methods proved successful and the Re-Ni electrodeposits spalled off of the substrate. We had similar results for a high temperature H13 tool steel. Considering the significant matrix of variable that were examined in the bath chemistry and electrodeposition process, there are as many variables also associated with surface preparation and alloy content. We did not explore this issue to the extent that we would have liked. In addition, flat samples were used rather than a complicated geometry.

We had success applying electrolessly Re-Ni and Re-Co to activated carbon, glassy carbon, reticulated vitreous carbon, carbon fibers, and carbon-carbon composites as seen in Figure 5.1. We also directly applied a Re-Ni coating to a carbon-carbon composite that did not have an electroless strike layer (Figure 5.2). The quality of the adhesion was not assessed on these samples

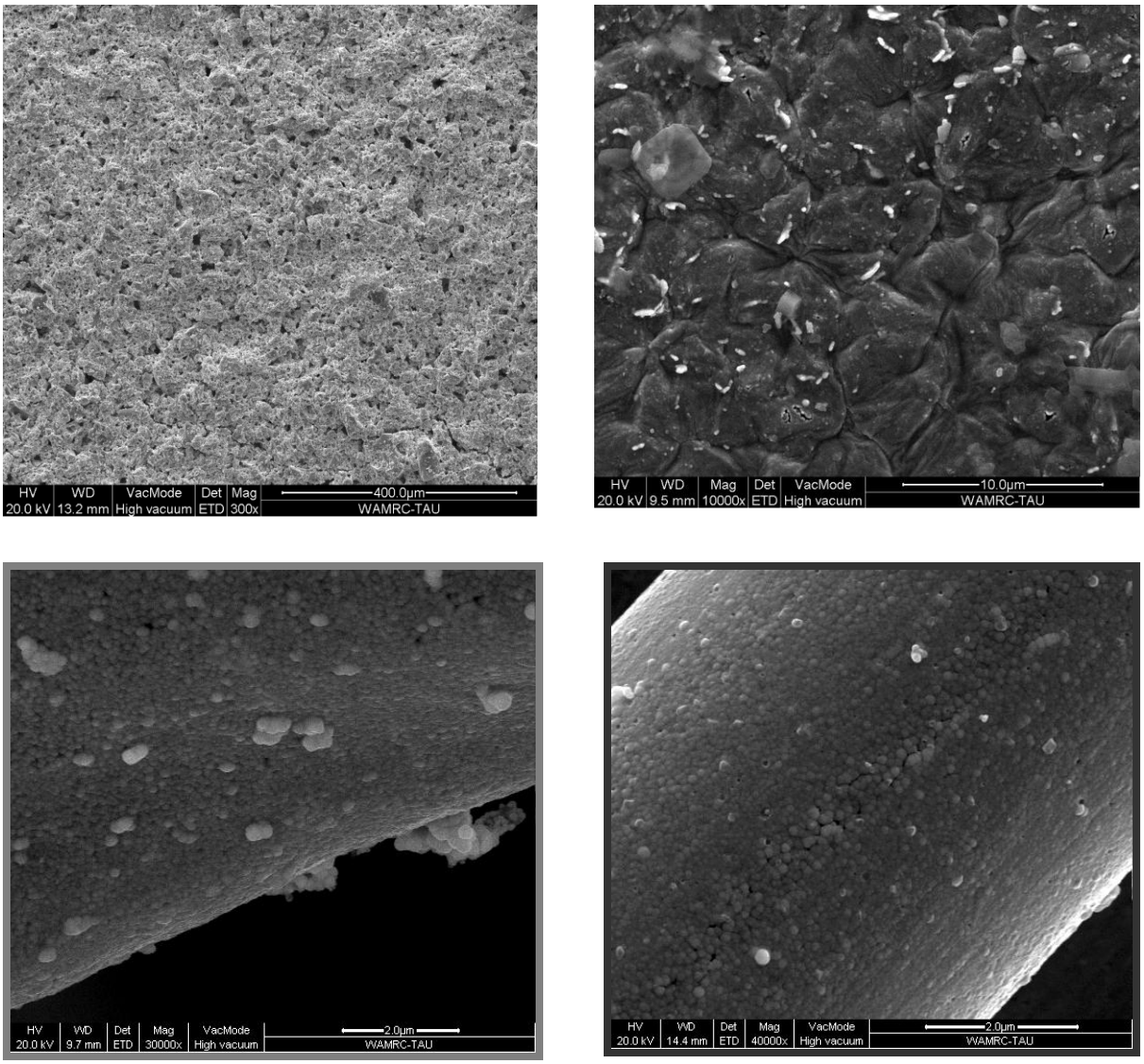

Figure 5.1. Electroless Re-Ni coatings applied to activated carbon (top left), glassy carbon (top right), reticulated vitreous carbon (bottom left), and carbon fiber (bottom right).

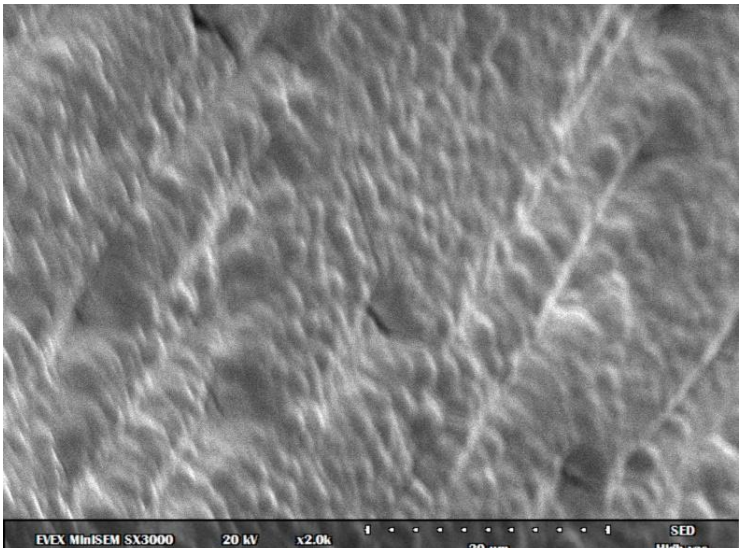

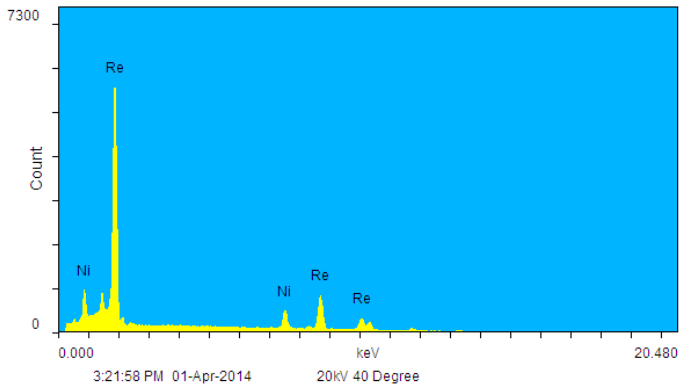

Figure 5.2. SEM (top) and EDS (bottom) of a direct Re-rich, Re-Ni electrodeposit on a carbon-carbon composite. No prior electroless strike layer was used.

6.0 PROPOSED APPROACHES NOT TAKEN

6.1 Vertical Scanning Interferometry (VSI)

It was proposed that both mechanistic and process information would be attained with a new one-of-a-kind interferometric system developed at Rice University (RU). UH proposed to collaborate with RU and use Super Resolution Vertical Scanning Resolution Interferometry (SRVSI) to examine nucleation and growth kinetics in a near-*in situ* cell. SRVSI has sub-angstrom vertical resolution, 50 nm (or less) lateral resolution, and a dynamic range that is 1000-times that of AFM. VSI was also proposed as method to quantify the surface morphology of deposits and aid in screening the quality of electrodeposits.

The faculty member at Rice University who developed SRVSI moved to the University of Bremen, so that we could no longer use SRVSI for the investigation of film nucleation, growth, and surface roughness. As we learned more about SRVSI, we determined that this method would have had limitations in its ability to resolve features of interest. While the super resolution interferometric aspect of this method could resolve sub-micron features in the z axis, the dimension of features in the x and y directions would have been limited by normal light optics, i.e. to ca. 10 μm.

We sought a work around to investigate these questions through the use of *ex situ* atomic force microscopy (AFM). *Ex situ* means that we would conduct the electrochemistry on a sample, extract it from solution, and then examine it in an AFM, while *in situ* AFM is when AFM is performed in solution while the electrochemistry is taking place or soon after. If we had success with *ex situ*, the plan was to then try *in situ*.

The first and most important decisions in the investigation of nucleation and growth kinetics is that of the substrate material and surface finish. This is where there is a departure from reality. While we want to know about the nucleation and growth kinetics on a substrate of interest, e.g., copper, much of the research in this area has been conducted on glassy carbon of silicon wafers. These later materials can be acquired with consistent, near atomistically smooth surface finishes. The lack of surface defects allows nucleation to be controlled by the applied energy. But the reality is that any real substrate will have surface defects over a range of dimensions that will control nucleation and growth. And these defects will not be consistent from sample to sample making it almost impossible to do a controlled experiment.

We first tried our experiments with single crystal copper. But we did not have consistent results. We then tried to vapor deposit copper onto mica. The proper approach would have been to use the mica side of the copper film. These experiments ran into logistical problems because they required us to travel to College Station and coordinate with personnel who were on a heavy travel schedule.

6.2 The development of high throughput electrodeposition methods

We proposed to create high throughput (HT) electrodeposition methods to allow full factorial experimental design, delineate relevant variables, and optimize bath chemistry,

additives, operating conditions, and pulse plating methods. The electrochemical instrumentation to perform 16 simultaneous, three-electrode, electrochemical experiments is available and was purchased through a DURIP acquired during this program. We also built the electrochemical cells and made appropriate Ag-AgCl reference electrodes. However, commercial instrumentation to provide multi-channel heating and stirring capability is sorely lacking in quality and availability. We could not find multi-channel stations that were capable of independent control of heating and/or stirring. The system that we purchased had four stations per unit and provided the same heat to all four stations, but allowed independent control of stirring. We purchased four of these systems so that we could conduct 16 simultaneous experiments. Three of the four systems that we purchased broke, were returned, broke again, were returned again, and broke for a final time. The four operating channels did not allow for full factorial experimental design.

It should be noted that this program also performed research above and beyond that which was originally proposed. We performed a significant amount of computational chemistry to understand the interactions between the bath components and between bath components and the substrate. While the catalytic nature of the transition metal ions were documented through experimental outcomes, and presence of complexes had been invoked, there had been no direct experimental proof of the presence of these complexes.

This research program developed the first computational evidence for the effect of the transition metals on the perrhenate cage. We also developed the first direct evidence that such complexes can exist following the addition of energy. This energy could come from the electrification of the metal interface.

To further verify this idea, we attempted to perform spectroelectrochemistry. The bonds of the species we were interested could only be detected in the infra-red portion of the spectra. In situ spectroelectrochemistry in the infrared is non-trivial, even for those that have spent careers in spectroscopy. The electrochemical cell and electrodes must be less than 20 μm in thickness to minimize the absorption of the IR light. We purchased the appropriate windows, spacers, electrodes, and designed a cell that would allow flow of reactants in and products out. We could not complete this phase of research due to time limitations.

6.3 Electrodeposition of Re and Re-M alloys on shapes of interest to the DoD

It was pointed out previously that this program was able to electrodeposit rhenium on substrate materials of interest to the DoD, e.g., carbon-carbon composites (CCC). Although not specified in the proposal, we also sought to assess the ability of these deposits to protect CCC and Si-C substrates at high temperature. We constructed CCC and SiC stubs in a form that could be used in the high temperature test facility at the University of Vermont. Unfortunately, we were not able to complete this task due to time and manpower constraints.

7.0 CONCLUSIONS AND SIGNIFICANT FINDINGS

This research program has provided significant insight into the electrodeposition and electroless deposition mechanism of Re-M alloys, a material that has strategically important wear, friction, corrosion, and nontoxic characteristics. Layered within our technical findings are the creation of novel experimental methods that can be used to understand other electrochemical systems. Perhaps even more important than all of this, is the education of a new generation of young scientists in a strategically important, yet unglorified, area of science. Some of the more important findings are:

7.1 Electrodeposition of Re-M alloys

- Metallic rhenium can be deposited from aqueous solutions of potassium or ammonium perrhenate ($KReO_4$ or NH_4ReO_4, respectively), but the deposit is non-uniform, the adhesion to the surface is poor, and the Faradaic efficiency (FE) is very low, hence this process is not likely to be of any practical importance.
- Adding even a very small concentration of an iron-group metal (M = Ni, Co or Fe) salt to the bath has a very strong catalytic effect.
- A unique mechanism of induced co-deposition was suggested, where the cation of the iron-group metal acts as a catalyst, namely a reducing agent that is formed and regenerated in-situ during the course of the reaction. It acts to reduce the most stable 7-valent perrhenate (ReO_4^-) anion to the less stable 5-valent rhenate (ReO_3^-) anion, which can then be reduced by electron and proton transfer.
- Computational methods show the interaction of the at the transition metal ion helps to open the perrhenate cage to expose the Re ion.
- The complexation of bath species was shown to occur when energy is added to the species.
- Electroplating baths were developed, with citric acid ($C_6H_8O_7$) as the complexing agent.
- Re-contents as high as 93 at.% or FE values as high as 96% were attained in different solutions. These values represent significant improvements compared to values previously reported by other investigators.
- The mass gain shows a linear dependence on time, indicating a uniform rate of deposition, regardless of the coating thickness. Re-Co deposition is the fastest (24 μm/h), Re-Ni deposition is the slowest (10 μm/h).
- Higher values of Re-content in the coating were typically associated with lower values of FE, i.e. a tradeoff must be made.
- Crack-free Re-Co and Re-Ni alloys were formed by pulse plating and by potentiostatic electrodeposition, with Re-contents in the deposits up to 82 at.%, and FE as high as 76%.

- In pulse plating, reverse pulse shape was found most useful for obtaining crack-free Re-Co alloys, while cathodic pulse plating shape was found helpful for obtaining crack-free Re-Ni alloys.
- Re-Ir-Ni coatings were developed. Re-Ir-Ni coatings as thick as 18 µm, with Re-content as high as 73 at.% and Ir-content as high as 37 at.%, were obtained, using different plating baths and operating conditions.
- The deposition of Ni^{2+} and Ir^{3+} are competing reactions occurring in parallel.
- The ternary Re-Ir-Ni system showed a phase separation. A mixture of HCP Re-Ir-based phase and HCP Ni phase with nanometric crystallites were observed. To the best of our knowledge, this is the first systematic observation of the electrochemical formation of the HCP Re-Ir-based phase.
- A mesoscale colony surface structure (also known as nodular, or cauliflower structure) was most common, with clear intercolony boundaries and surface grooves. Each colony consists of hundreds of small grains. The appearance of these 3D islands indicates on a Volmer-Weber (VW) growth mode.
- A unique combination of banded (multilayer) and columnar structure was observed by aberration corrected TEM and Atom Probe Tomography (APT). This was done in collaboration with Northwestern University and the University of Chicago. The banded structure consists of Ni-rich and Re-rich layers. Hetero-epitaxial growth results in very high intrinsic stresses and residual shear strains, which may be the cause of micro-cracks.
- Electrodeposition of Re-Ni alloys was studied also at very short times (0.05 - 60 seconds). Anomalously high FE was observed at short times, well above 100%, indicating that some chemical reduction of the perrhenate ion occurs in parallel to electroplating. Both the FE and Re-content decreased with increasing deposition time.
- Weak ionic interactions on electrode reactions during electrodeposition of Re-Ni alloys were observed. It was concluded that the induced co-deposition of rhenium and nickel proceed partially from a precursor adsorbed on the cathode and is partially due to the deformed ReO_4^- and Ni^{2+}-citrate ions. The deposition from this precursor leads to formation of the layer catalyzing parallel deposition from perrhenate ion and Ni-citrate complex separately.
- The microstructure and composition of pulse plated Re-Ni alloys from Ni-rich electrolytes were studied. At low duty cycle and high frequency, Re deposition was activation controlled. The Re-content in the coating increased with decreasing pulse time until the region of activation control was reached. The limiting current density in the activation regime of pulse plating showed dependence on the concentration of citrate; therefore, the rate-limiting step appears to be the formation of a citrate complex. At high citrate concentrations – the limiting current flattens out and the mutli-step surface reduction of oxides becomes the limiting step(s). Short duty cycles gave a lower concentration of rhenium alloy oxides compared to larger duty cycles. In the context of our

proposed mechanism, this suggests that the electroless reduction of rhenium oxides takes place at a faster rate during the relaxation time.

- The deposition of Re-Ni alloys from additive-containing baths was studied. The main objective was to find suitable bath additives that would reduce the formation of surface cracks. The use of sodium lauryl sulfate, glycine, vanillin, coumarin, EDTA, triethanolamine and polyethylene glycol resulted in an increase of the Re-content of the alloy and/or the FE. Gelatin was found to have a significant influence on the surface morphology and cracking pattern. The lowest crack density was achieved when a mixture of three additives were used.

7.2. Electroless plating of Re-M alloys

- An electroless plating was developed for Re-M alloys, where M is an iron-group metal. Different substrates were used: pure copper foils, sputtered copper (75 nm) on TaN/SiO_2/Si, SiO_2(100 nm)/Si, activated carbon, vitreous (glassy) carbon, carbon fibers, and carbon-carbon composite. They represent metallic, semiconducting and electrically insulating surfaces. Films containing as high as 90 at.% Re were obtained.
- A catalytic effect of the iron-group metals similar to that reported for electrodeposition was also found in the case of electroless plating.
- The early stages of growth of ultrathin (<20 nm) Re-Ni films with high Re-content by electroless plating on a functionalized-SiO_2 substrate were studied. The addition of a low concentration of Ni^{2+} ions to the electrolyte was found necessary to obtain full surface coverage and thicker deposits. The Re-content was not uniform along the thickness of the deposit, and had a maximal value at the percolation point. The deposition process was found to consist of sequential reduction reactions, from ReO_4^- to lower valence oxides, such as ReO_3 and ReO_2, to metallic Re.

8.0 PERSONNEL SUPPORTED

M.Sc. Students with Thesis

02/10–5/12 Maayan Cohen-Sagiv, “Electrochemical Deposition of Re-Ir Coatings,” Materials and Nanotechnologies Program, TAU, won a Dean scholarship for excellent graduate students.

09/12–03/15 Tzippora Nusbaum, “Effect of Pulse On-Time and Peak Current Density on Pulse Plated Re-Ni Alloys,” Materials Science and Engineering, TAU.

Ph.D. Students

11/08–06/12 Adi Naor-Pomerantz, “Electrodeposition of Rhenium-Based Coatings for Aggressive Environments,” Materials Science and Engineering Program, TAU, won the Center for Nanoscience and Nanotechnology scholarship for excellent Ph.D. students, won 3rd place poster presentation award at EMNT 2010 – The 8th Int. Symp. on Electrochemical Micro & Nanosystem Technologies, Cannes Mandelieu, France. Title: “Electrodeposition of alloys of rhenium with the iron-group metals: Mechanism study”.

01/09–present Alla Duhin, “Electroless Deposition of Rhenium-Based Alloys,” passed candidacy exam on 30/04/2012. Won the 2012/3 Israel Ministry of Science and Technology scholarship for promotion of excellent female graduate students in science.

Post-Doctoral Research Assistants

2013–2014 Dr. Brian A. Rosen, “Rhenium Alloy Electrodeposition: Towards Crack-Free Coatings and Understanding the Mechanisms,” Post-Doctoral Fulbright Scholar and TAU's Nanocenter Scholar, TAU.
Current Position: Senior Lecturer, Department of Materials Science and Engineering, Tel-Aviv University, Israel.

2013–2014 Dr. Wangping Wu, “Electroplating of Rhenium-Base Alloys,” Post-Doctoral Pikovsky Valazzi Scholar, TAU.
Current Position: Senior Lecturer, School of Mechanical Engineering, Changzhou University, Jiangsu Province, China.

2010-2014 Dr. Francesco Contu, “Further Insight into the Mechanism of Re-Ni Electrodeposition from Concentrated Citrate Baths”, Post-doctoral Research Assistant, UTHSC, TEES.
Current Position: Assistant Instructional Professor, Department of Chemistry, California State Polytechnic Institute, Pomona, CA.

2012-2014 Dr. Sujit Mondal, “The Rapid Identification and Characterization of Organic Corrosion Inhibitors: Correlation of Experimental Results with a New Experimental Model”, Post-doctoral Research Assistant, UTHSC, TEES. Current Position: Corrosion Specialist, Exova, Inc., Houston, TX

2012-2014 Dr. Manuel Vega-Arroyo, “DFT Investigation of the Structure and Electrochemical Properties Resulting from Interaction between Perrhenate, Citrate Ion and Nickel-Citrate Complexes”, UTHSC, TEES. Current Position: Research Assistant Professor, College of Technology, University of Houston, Houston, TX.

9.0 PUBLICATIONS AND PRESENTATIONS

S.R. Taylor, N. Eliaz and E. Gileadi
Grant No. FA9550-10-1-0520

9.1 Publications

2010

1. A. Naor, N. Eliaz, L. Burstein and E. Gileadi, "Direct Experimental Support for the Catalytic Effect of Iron-Group Metals on Electrodeposition of Rhenium," *Electrochemical and Solid-State Letters*, **13**(12) (2010) D91-D93.
2. A. Naor, N. Eliaz and E. Gileadi, "Electrodeposition of Alloys of Rhenium with Iron-Group Metals from Aqueous Solutions," *Journal of the Electrochemical Society*, **157**(7) (2010) D422-D427.
3. A. Naor, N. Eliaz and E. Gileadi, "Electrodeposition of Alloys of Rhenium with Iron-Group Metals from Aqueous Solutions," *Electrochemical Society Transactions*, **25**(29) (2010) 137-149.
4. A. Naor, N. Eliaz, E. Gileadi and S.R. Taylor, "Properties and Applications of Rhenium and Its Alloys," *The AMMTIAC Quarterly*, **5**(1) (2010) 11-15.

2011

5. A. Duhin, A. Inberg, N. Eliaz and E. Gileadi, "Electroless plating of rhenium-nickel alloys," *Electrochimica Acta*, **56** (2011) 9637-9643.
6. A. Naor-Pomerantz, N. Eliaz and E. Gileadi, "Electrodeposition of Rhenium-Tin Nanowires," *Electrochimica Acta*, **56** (2011) 6361-6370.
7. A. Naor-Pomerantz, N. Eliaz and E. Gileadi, "Formation of Sn–Core/Re–Shell Nanowires Electrochemically," in Proc. TechConnect World Conference and Expo 2011, Nanotech 2011, Vol. 1, Chapter 4, pp. 419–420 (Boston, MA, June 13 – 16, 2011).
8. S.R. Taylor, "The Investigation of Corrosion Phenomena with High Throughput Methods: A Review", *Corrosion Reviews,* **29**(3-4):135–151 (2011).

2012

9. F. Contu and S.R. Taylor, "Further Insight into the Mechanism of Re-Ni Electrodeposition from Concentrated Citrate Baths", *Electrochimica Acta*, **70**:34-41 (2012).

2013

10. M. Cohen Sagiv, N. Eliaz and E. Gileadi, "Incorporation of iridium into electrodeposited rhenium-nickel alloys," *Electrochimica Acta*, **88** (2013) 240-250.

2014

11. S.K. Mondal and S.R. Taylor, "The Rapid Identification and Characterization of Organic Corrosion Inhibitors: Correlation of Experimental Results with a New Experimental Model", *J. Electrochem. Soc.,* **161**(10)C476-C485 (2014).

12. O. Berkh, N. Eliaz and E. Gileadi, "The Initial Stages of Electrodeposition of Re-Ni Alloys," *Journal of the Electrochemical Society*, **161**(5) (2014) D219-D226.
*** The first open-access manuscript of the Electrochemical Society.
13. A. Duhin, A. Rozenblat-Raz, L. Burstein, A. Inberg, D. Horvitz, Y. Shacham-Diamand, N. Eliaz and E. Gileadi, "Growth Study of Nanoscale Re-Ni Coatings on Functionalized SiO2 using Electroless Plating," *Applied Surface Science*, **313** (2014) 159-165.
14. O. Berkh, A. Khatchatouriants, N. Eliaz and E. Gileadi, "The Influence of Weak Ionic Interactions on Electrode Reactions during Electrodeposition of Re-Ni Alloys," *Journal of the Electrochemical Society*, **161**(12) (2014) D632-D639.
15. B.A. Rosen, E. Gileadi and N. Eliaz, "Microstructure and Composition of Pulse Plated Re-Ni Alloys on a Rotating Cylinder Electrode," *Journal of Electroanalytical Chemistry*, **731** (2014) 93-99.

2015

16. W. Wu, N. Eliaz and E. Gileadi, "The Effects of pH and Temperature on Electrodeposition of Re-Ir-Ni Coatings from Aqueous Solutions," *Journal of the Electrochemical Society*, **162**(1) (2015) D20-D26.
17. T. Nusbaum, B.A. Rosen, E. Gileadi and N. Eliaz, "Effect of Pulse On-Time and Peak Current Density on Pulse Plated Re-Ni Alloys," *Journal of the Electrochemical Society*, **162**(7) (2015) D250-D255.
18. A. Duhin, A. Inberg, N. Eliaz and E. Gileadi, "Electroless Plating of Rhenium-Based Alloys with Nickel, Cobalt and Iron," *Electrochimica Acta*, **174** (2015) 660-666.

Manuscripts in Preparation or Review

1. M. Vega-Arroyo, F. Contu, and S.R. Taylor, "DFT Investigation of the Structure and Electrochemical Properties Resulting from Interaction between Perrhenate, Citrate Ion and Nickel-Citrate Complexes", *Journal of Chemical Physics* (in review).
2. Sung-Il Baik, A. Duhin, P.J. Phillips, R.F. Klie, E. Gileadi, D.N. Seidman and N. Eliaz, "A Correlative Atomic-Scale Study of the Combined Multilayer and Colony Structure of an Electrodeposited Re-Ni Coating for High-Temperature Applications."
3. W. Wu, N. Eliaz and E. Gileadi, "Electrodeposition of Re-Ni Alloys from Aqueous Solutions: The Effect of Bath Additives."
4. O. Berkh, L. Burstein, A. Gladkikh, N. Eliaz and E. Gileadi, "Study of the Catalytic Growth of Thin Electrodeposited Re-Ni Films by TOF-SIMS and HR-XPS."

9.2 Presentations

2010

1. N. Eliaz, A. Naor, A. Duhin, A. Inberg and E. Gileadi, "Electroplating and electroless deposition of rhenium-based alloys," The 8th Int. Symp. on Electrochemical Micro & Nanosystem Technologies – EMNT 2010, Cannes Mandelieu, France, September 21 – 24 (2010). (**invited**)
2. A. Naor, N. Eliaz and E. Gileadi, "Electrodeposition of alloys of rhenium with the iron-group metals: Mechanism study," The 8th Int. Symp. on Electrochemical Micro & Nanosystem Technologies – EMNT 2010, Cannes Mandelieu, France, September 21 – 24 (2010). *** Recipient of the Third Best Poster Presentation Award.

3. A. Duhin, A. Inberg, N. Eliaz and E. Gileadi, “Thin film coating of rhenium alloys prepared by electroless deposition,” The 8th Int. Symp. on Electrochemical Micro & Nanosystem Technologies – EMNT 2010, Cannes Mandelieu, France, September 21 – 24 (2010).
4. A. Naor, N. Eliaz and E. Gileadi, “Study of the electrodeposition mechanism of alloys of rhenium with the iron-group metals,” The 61st Annu. Meeting of the Int. Soc. of Electrochemistry: Electrochemistry from Biology to Physics, Nice, France, September 26 – October 1 (2010).
5. A. Duhin, A. Inberg, N. Eliaz and E. Gileadi, “Electroless deposition of rhenium alloys,” The 61st Annu. Meeting of the Int. Soc. of Electrochemistry: Electrochemistry from Biology to Physics, Nice, France, September 26 – October 1 (2010).
6. A. Naor-Pomerantz, N. Eliaz and E. Gileadi, “Electroplating of rhenium – iron group metal alloys: Mechanism, properties and applications,” The 9th Biannu. Conf. of the Corrosion Forum, Kfar Maccabiah, Ramat Gan, Israel, November 10 (2010).
7. S.R. Taylor, “Technology Transfer between the Silos: *Rhenium and Beyond”,* in the panel discussion “Corrosion: The Biggest Challenge for the Energy Industry” , The Emerging Energy Technologies Conference, Rice University, Houston, TX August 2010 (**invited**).
8. S.R. Taylor, “Corrosion and Durability Issues in Medical Implants and Devices”, a two hour lecture series, Osteomed, L.P., Addison, TX, August 2010 (**invited**)
9. S.R. Taylor, “The Prediction of Long-term Field Performance of Coatings Using Rapid Laboratory Tests” , Metal Protection through Coatings Technology Conference, American Coatings Association, Pittsburgh, PA ,October 2010 (**invited**)
10. S.R. Taylor, “Understanding Materials through Electrochemical Measurements”, BD Technologies, Research Triangle Park, NC, October 2010 (**invited**) .

2011

11. M. Cohen-Sagiv, N. Eliaz and E. Gileadi, “Electroplating of Re-Ir based alloys from aqueous solutions,” Israelectrochemistry, Jerusalem, Israel, June 23 (2011).
12. S.R. Taylor, “Corrosion Prevention Systems: Predicting Performance, Assessing Quality”, Materials Technology Institute AmeriTAC 104 Meeting, San Antonio, TX, February 2011.(**invited**)
13. S.R. Taylor**,** “Corrosion Mitigation: the Prediction of Performance and the Discovery of New Materials”, BP America, Houston, TX , May 2011. (**invited**)
14. S.R. Taylor, “Corrosion Mitigation: the Prediction of Performance and the Discovery of New Materials”, Chevron, Houston, TX, June 2011. (**invited**)
15. S.R. Taylor, ““Understanding and Discovering Materials through Electrochemical Methods” , 26th Congress of the Mexican Society for Electrochemistry, Mexico City, Mexico**, Plenary Lecture,** June 2011 (**invited**).

2012

16. N. Eliaz, A. Naor-Pomerantz, A. Duhin, A. Inberg and E. Gileadi, “Electroplating and electroless plating of rhenium and its alloys,” CORROSION 2012, Salt Lake City, UT, March 11 – 15 (2012). (**invited**)

17. N. Eliaz, A. Naor-Pomerantz, A. Duhin, M. Cohen-Sagiv and E. Gileadi, “Electroless and electrochemical deposition of rhenium and its alloys,” The 3rd Conf. for Materials and Processes 2012, Ramat Gan, Israel, May 14 (2012). (**invited**)
18. A. Duhin, A. Inberg, N. Eliaz and E. Gileadi, “Electroless plating of rhenium base alloys with the iron-group metals,” The 9th Int. Symp. on Electrochemical Micro & Nanosystem Technologies – EMNT 2012, Linz, Austria, August 15 – 17 (2012).
19. S.R. Taylor, “Technology Transfer between the Silos: *Rhenium and Beyond”,* presented in the workshop on “The A-Z of Corrosion Fundamentals and How to Measure the True Cost of Corrosion in Asset Life Cycle Management” in the Conference “Corrosion Management for Oil and Gas”, Houston, TX, December 10-12, 2012. (**invited**)
20. S.R. Taylor, “The Discovery and Understanding of Materials Using Electrochemical Methods”, Texas A&M University, School of Engineering, College Station, TX, August 2012
(**invited**).
21. S.R. Taylor, “Using Electrochemical Methods to Model, Understand, and Discover Coating Materials”, Rice University, Dept. of Mech. Engr. & Matl. Sci., Houston, TX, October, (**invited)**

2013

22. A. Duhin, A. Rozenblat-Raz, A. Inberg, D. Horvitz, Y. Shacham-Diamand, N. Eliaz and E. Gileadi, “Formation of Nanoscale Re-Ni Coatings on SiO2 Substrate Using Electroless Plating,” Materials for Advance Metallization 2013 — MAM 2013, Leuven, Belgium, March 10 – 13 (2013).
23. A. Duhin, A. Inberg, N. Eliaz and E. Gileadi, “Electroless Plating of Rhenium Base Alloys with Nickel, Cobalt and Iron,” The 223rd ECS Meeting, Toronto, Canada, May 12 – 17 (2013).
24. N. Eliaz, “Electroplating and Electroless Plating of Rhenium and its Alloys,” University of Illinois at Urbana-Champaign, Champaign, IL, 10/4/2013.
25-29. S.R. Taylor, “Using Electrochemical Methods to Model, Understand, and Discover Materials”, Shell Oil, Pioneer Natural Resources, Halliburton, PM&AM, Formosa Plastics,

2014

30, 31. S,K, Mondal and S.R. Taylor, “Modeling Corrosion Inhibition Using Quantum Theory of Atoms in Molecules”, Presented at (1) Research in Progress Symposium and (2) Symposium on State-of-the-Art Research in Corrosion Inhibitors (**invited**). National Association of Corrosion Engineers, San Antonio, March 2014.
32. N. Eliaz, B.A. Rosen and E. Gileadi, “Electroplating of Rhenium-Based Alloys for High Temperature and Catalytic Applications,” Material Technologies and Modeling – The 8th Int. Conf., Ariel, Israel, July 28 – August 1 (2014). **KEYNOTE lecture**
33. A. Duhin, A. Inberg, N. Eliaz and E. Gileadi, “Formation of Re-Ni and Re-Co Coatings using Electroless Plating for High-Temperature Applications,” The 16th Israel Mater. Eng. Conf. — IMEC-16, Technion, Israel, February 23 – 25 (2014).

34. O. Berkh, L. Burstein, N. Eliaz and E. Gileadi, “The Initial Stages of Electrodeposition of Ni-Re Alloys,” The 16th Israel Mater. Eng. Conf. — IMEC-16, Technion, Israel, February 23 – 25 (2014).
35. O. Berkh, N. Eliaz and E. Gileadi, “The Electrodeposited Re-Ni alloys and the Early Stages of their Deposition,” 65th Annual Meeting of the Int. Society of Electrochemistry, Lausanne, Switzerland, August 31 – September 5 (2014).
36. O. Berkh, A. Khatchatouriants, N. Eliaz and E. Gileadi, “Ionic Interaction in Citrate Electrolyte for Deposition of Re-Ni Alloys and the Mechanism of Deposition Process,” Israelectrochemistry 2014, Technion, Haifa, September 16 (2014).
37. T. Nusbaum, B.A. Rosen, E. Gileadi and N. Eliaz, “Microstructure and Composition of Pulse Plated Re-Ni Alloys on a Rotating Cylinder Electrode,” The 10th Biannu. Israeli Conf. of the NACE Int. Corrosion Forum in Israel — CFRI 2014, Ramat Gan, Israel, December 11 (2014).

2015

38. S.R. Taylor, “The Discovery of Materials Using Electrochemical Methods: An Invitation to Collaborate”, Royal Institute of Technology, Division of Chemistry and Chemical Engineering, Stockholm, Sweden**,** presented at faculty retreat in Djorönäset. January 15, 2015 (**invited**)

10.0 PATENT APPLICATIONS AND INVENTION DISCLOSURES

1. N. Eliaz, E. Gileadi and A. Naor, “Rhenium Nanostructures,” US patent application 2012/0122657 A1, May 17, 2012.
2. Invention Disclosure, S.R. Taylor and F. Contu, “A Mechanically-Assisted Electro-deposition Method to Increase the Adhesion of Electroplated Metals and Alloys on Any Metal Substrate”, submitted to University of Houston on 5/14/15.